Design of Oceanographic Surface Moorings for Harsh-Weather Environments

Mark A. Grosenbaugh, Visitor (Woods Hole Oceanographic Institution, Woods Hole, MA) and
Spyros A. Mavrakos, Visitor (National Technical University, Athens, Greece)

ABSTRACT

A comprehensive methodology is presented for designing instrumented oceanographic surface moorings for harsh weather environments. In the past, the design of oceanographic moorings was based on static analysis as most systems were deployed in regions where wave forcing was small. But now, many surface moorings are being placed in ocean environments where the predominant forcing is from waves and where the major cause of failure is cyclic fatigue. Here, dynamic analysis becomes as important as the static calculations. In this paper, we present the equations and numerical solution techniques for the statics and dynamics of a buoy/cable system with attached instruments. Hydrodynamic coefficients and wave exciting forces of different shaped oceanographic buoys are given along with the material parameters for the components and instruments that make up the mooring line. We show how to combine the results of the static and dynamic analysis with data from laboratory strength and fatigue tests of mooring components to predict if the mooring will survive the deployment. We present an analytical model of the dynamics of the mooring system that gives almost identical results with the numerical simulation and can be used during preliminary design. A comprehensive design example using the 1995 Arabian Sea surface mooring is presented to illustrate the design procedure.

INTRODUCTION

Oceanographers rely heavily on single-point surface moorings with attached instruments to make measurements of current, temperature, conductivity, light transmissibility, fluorescence, and other scientific quantities in the water-column. No other technique exists that can provide these measurements close to the surface and simultaneous with meteorological measurements above the surface. This is important to scientists who are studying the relationship between atmospheric forcing and ocean response. Surface moorings also allow scientists to receive data in real time via satellites.

The history of oceanographic surface moorings at Woods Hole Oceanographic Institution (WHOI) dates back 35 years. At that time, oceanographers envisioned a mooring with attached current meters that would be low cost and could be deployed easily from a small ship in water depths that ranged from 2000 m to over 5000 m. Their initial deployments, however, showed how difficult it was to maintain a small surface mooring for periods greater than two months (Richardson *et al.*, 1963). Failure rates were high with the principle causes being kinks forming in wire-rope mooring line, corrosion of the wire rope, fish biting through synthetic mooring line, and breaking of steel mooring hardware.

A major engineering study in the late 1960's and early 1970's (Berteaux and Walden, 1970) addressed these failures and led to the design of the WHOI taut surface mooring (Fig. 1a) which became a prototype for deploying instrumentation in deep ocean environments (Berteaux, 1976). The design consists of a combination of chain and wire rope in the upper 1500-2000 meters to protect against fish bites and nylon rope in the lower part of the mooring to give compliance. The wire rope uses a 3×19 torque-balanced construction to prevent kinking. It is galvanized and rubber coated to prevent corrosion. The ends of the wire rope, where it attaches to the instrument cages, are swaged into stainless-steel fittings and covered with

DTIC COULD NOT GET MISSING

PAGE FROM CONTRIBUTOR

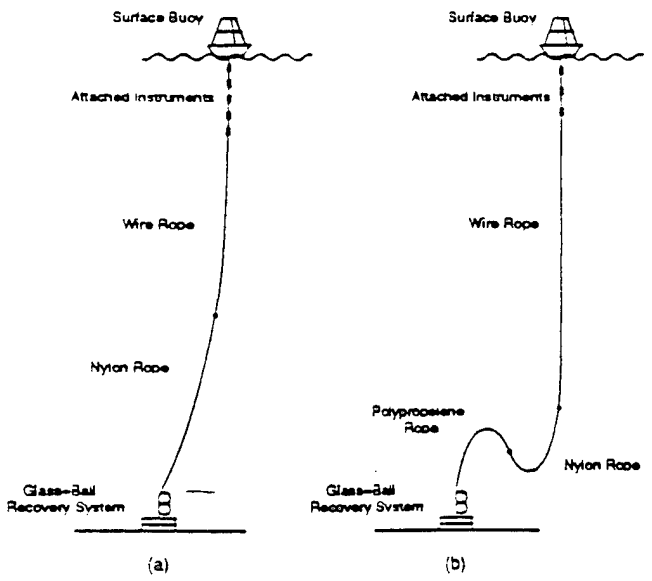

Figure 1: (a) Taut oceanographic surface mooring consisting of an upper string of instruments, wire rope, and a lower section of nylon rope that allows the mooring to stretch in strong currents. (b) Inverse-catenary mooring that has an extra section of polypropylene rope near the bottom to increase scope and reduce mean tension in currents.

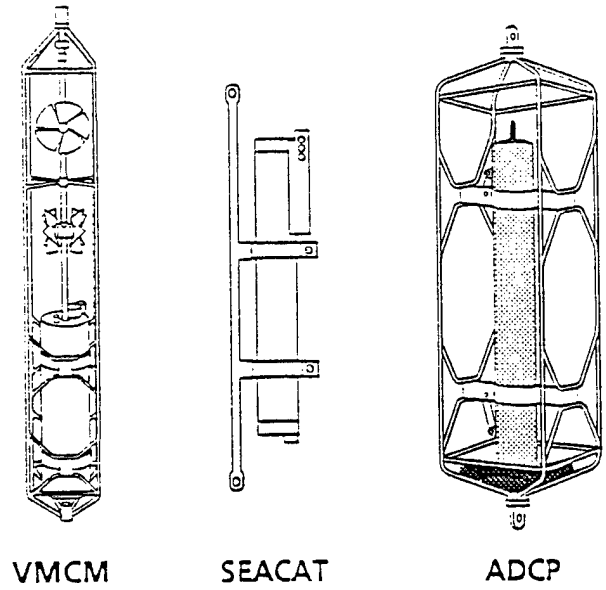

Figure 2: Instrumentation for oceanographic surface moorings. (a) Vector Measuring Current Meter (VMCM) for measuring current speed and direction, (b) SEACAT for measuring conductivity and temperature, (c) Acoustic Doppler Current Profiler (ADCP) for measuring current profile.

water-tight polyurethane boots. At the bottom of the mooring is a recovery system that uses an acoustically controlled release placed under a string of positively buoyant 17-inch diameter glass spheres. When released, the glass spheres float to the surface allowing for retrieval of all the instruments. The anchor and anchor tackle remain on the bottom. The size of the anchor is chosen so that it will lift off the bottom (allowing the mooring to drift) before the surface buoy is pulled underwater. The advantages of the taut mooring are that it has a small watch circle and the attached instruments are kept nearly vertical. The disadvantage is that, in strong currents, the mean tensions can become large enough so that the mooring will drift. Also, as we show later, the taut mooring can experience high dynamic in large sea states.

The instruments are attached in-line on the mooring, usually being concentrated in the upper chain/wire-rope section of the mooring line. On some moorings, there have been as many as 15 scientific and engineering instruments. On WHOI moorings, the workhorse instrument is the Vector Measuring Current Meter (VMCM) (Weller and Davis, 1980) and more, recently, an acoustic doppler current profiler (ADCP). In both of these, the electronics are placed in pressure-resistant housings and suspended in a cage made of 3/4-inch diameter stainless-steel rod. Other types of instruments have been placed in cylindrical pressure housings and attached to a single 1-1/4-inch diameter stainless-steel rod which acts as the strength member (Fig. 2). The steel cages and rods are attached to the chain or the swage fittings at the end of the wire rope using galvanized steel shackles and links (Fig. 3).

A variation of the taut mooring is the *inverse-catenary* mooring (Fig. 1b). The design was originally proposed in the late 1950's for mooring the Navy Oceanographic Meteorological Automatic Device (NOMAD) buoy (Berteaux, 1976). Since then, it has been used extensively by the National Data Buoy Center (Canada and May, 1985) for their offshore weather moorings. More recently, the *inverse-catenary* mooring has been adapted for deploying oceanographic instrumentation in severe current and wave environments. In this design, a piece of positively buoyant

REPORT DOCUMENTATION PAGE

Form Approved
OMB No. 0704-0188

1. AGENCY USE ONLY (Leave blank)	2. REPORT DATE	3. REPORT TYPE AND DATES COVERED
	1995	TECHINICAL

4. TITLE AND SUBTITLE

Design of oceanographic surface morrings for harsh-weather environments

5. FUNDING NUMBERS

ONR N00014-92-J-1269
ONR N00014-93-1-0704

6. AUTHOR(S)

Mark A. Grosenbaugh, and Spyros A. Mavrakos

7. PERFORMING ORGANIZATION NAME(S) AND ADDRESS(ES)

WOODS HOLE OCEANOGRAPHIC INSTITUTION
WOODS HOLE, MA 02543

8. PERFORMING ORGANIZATION REPORT NUMBER

WHOI CONTR. 9062

9. SPONSORING/MONITORING AGENCY NAME(S) AND ADDRESS(ES)

OFFICE OF NAVAL RESEARCH
ENVIRONMENTAL SCIENCES
DIRECTORATE
ARLINGTON, VA 22217-5660

10. SPONSORING/MONITORING AGENCY REPORT NUMBER

11. SUPPLEMENTARY NOTES

In citing this report in a bibliography, the reference given should be:

Proceedings of the 1995 103rd Annaul Meetingof the Society of Naval Architects and Marine Engineers, Washington, DC :395-423, 1995

12a. DISTRIBUTION/AVAILABILITY STATEMENT

APPROVED FOR PUBLIC RELEASE:
DISTRIBUTION UNLIMITED

12b. DISTRIBUTION CODE

13. ABSTRACT (Maximum 200 words)

A comprehensive methodology is presented for designing instrumented oceanographic surface moorings for harsh weather environments. In the past, the design of oceanographic moorings was based on static analysis as most systems were deployed in regions where wave forcing was small. But now, many surface moorings are being placed in ocean environments where the predominant forcing is from waves and where the major cause of failure is cyclic fatigue. Here, dynamic analysis becomes as important as the static calculations. In this paper, we present the equations and numerical solution techniques for the statics and dynamics of a buoy/cable system with attached instruments. Hydrodynamic coefficients and wave exciting forces of different shaped oceanographic bodies are given along with the material parameters for the components and instruments that make up the mooring line. We show how to combine the results of the static and dynamic analysis with data from laboratory strength and fatigue tests of mooring components to predict if the mooring will survive the deployment. We present an analytical model of the dynamics of the mooring system that gives almost identical results with the numerical simulation and can be used during preliminary design. A comprehensive design example using the 1995 Arabian Sea surface mooring is presented to illustrate the design procedure.

14. SUBJECT TERMS

1) surface morrings
2) oceanographic moorings
3) mooring dynamics

15. NUMBER OF PAGES
29

16. PRICE CODE

17. SECURITY CLASSIFICATION OF REPORT	18. SECURITY CLASSIFICATION OF THIS PAGE	19. SECURITY CLASSIFICATION OF ABSTRACT	20. LIMITATION OF ABSTRACT
UNCLASSIFIED	UNCLASSIFIED	UNCLASSIFIED	

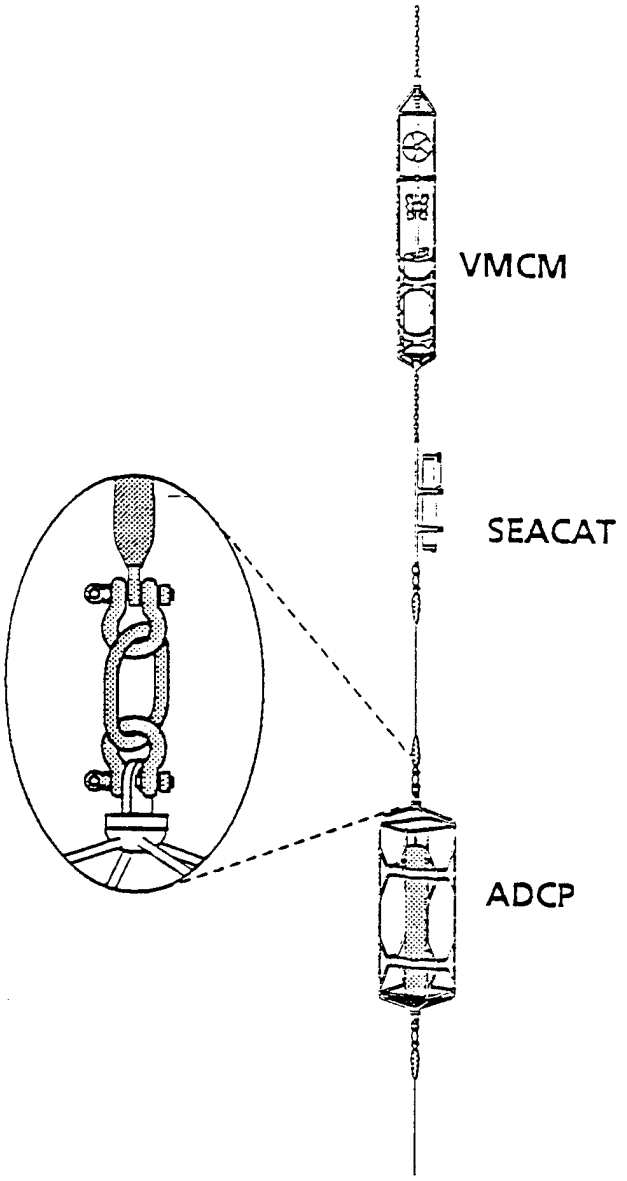

Figure 3: Instruments attached in-line on the mooring with shackles and oval end links.

polypropylene rope is inserted near the bottom, just above the glass-ball recovery system, in order to increase scope and at the same time prevent tangling of excess line around the glass-ball recovery system. The extra scope helps to reduce static tensions through changes in the geometry of the mooring line rather than through stretching. However, hydrodynamic damping constrains geometrical changes at higher wave frequencies (Triantafyilou, 1987) so that

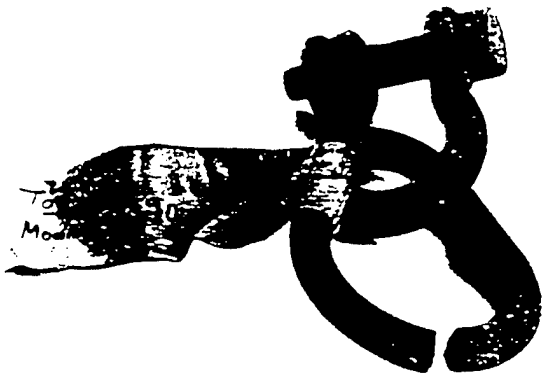

Figure 4: Fatigue failure of 5/8-inch pear-shaped sling link on the 1989 MLML mooring.

the dynamic response is similar to that of the taut oceanographic surface mooring.

The success of WHOI surface moorings during oceanographic experiments of the 1980's can be attributed to a systematic design procedure that was developed for analyzing the static configuration of a mooring in currents (Berteaux, 1991). The success can also be attributed to the fact that these early deployments (Briscoe and Weller, 1984; Weller *et al.*, 1990) took place in environments that, except for isolated storms, experienced small sea states. However, there has been a push in the past few years to deploy oceanographic surface moorings in harsh-weather environments. Areas in the North Atlantic and in the Arabian Sea which experience high winds and large seas a significant portion of the time have been sites of recent moorings. One mooring in particular, the 1989 *Marine-Light, Mixed-Layer* (MLML) taut surface mooring deployed 400 km south of Iceland (Pleuddemann *et al.*, 1995), highlighted the need for incorporating dynamic analysis into the design process. This mooring parted after 70 days when a 5/8-inch galvanized-steel sling link placed at the top of the mooring line failed in fatigue (Fig. 4). This is in spite of the static analysis that predicted the component could easily withstand the maximum expected loads.

What was missing in the analysis of the 1989 MLML mooring was a procedure for predicting dynamic tensions and fatigue in mooring line components. Because of the compliance built into taut and inverse-catenary moorings through the synthetic rope, the instrument string is free to accelerate up and down

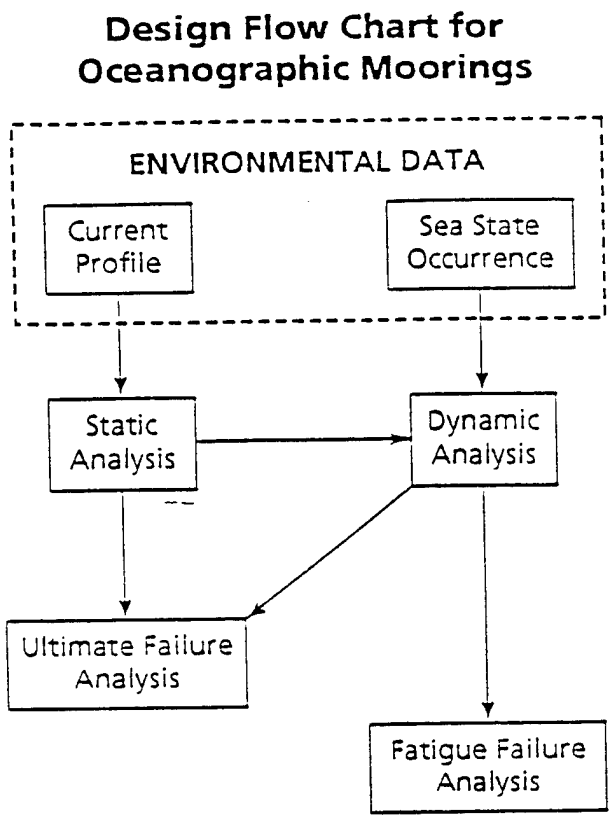

Figure 5: Flow chart showing how static and dynamic analysis are combined into ultimate-strength and fatigue analysis.

nearly in phase with the buoy. Depending on the total mass of the instruments and the amplitude and frequency of the waves, large dynamic tensions can result at the top of the mooring line. These oscillatory loads can be of similar magnitude to the static loading, and they are applied over and over again as many as 10 million times during a one-year deployment. Even in relatively benign wave environments where the goal is to maintain a mooring for up to one year, dynamic tensions can play a major role in the survival. This was made clear when two moorings of the 1993 *Subduction* experiment, deployed 1200 km west of the Canary Islands, parted when titanium current meter cages failed in fatigue at weld joints.

The goal of this paper is to present a comprehensive methodology for designing instrumented oceanographic surface moorings for harsh weather environments that takes into account the effects of both static and dynamic loading. The important point here is that by incorporating dynamic loading we are able to estimate fatigue life and to make more accurate predictions of extreme tensions which are a combination of static and dynamic tension. Fig. 5 gives a flow diagram of how we view the design process. The main steps are characterizing the ocean environment in terms of wind, waves, and current. This is followed by static and dynamic analysis for predicting the different loads that a mooring component is likely to experience. Finally, using the material properties along with safety factors, appropriate components are selected that can resist both the extreme loads which cause ultimate failures and the cyclic loads which are responsible for fatigue failures.

While the offshore industry is well versed in many of the areas that we address in this paper, the oceanographic community has ignored these concepts in the design of their moorings. One of the reason's for this is today's oceanographic engineers are required to perform a wide variety of jobs. Besides designing moorings, they design and build instruments that go on the moorings, and they go to sea to supervise deployment and recovery. Because of these demands, it is very difficult for them to specialize in dynamic analysis and fatigue analysis. And because of costs, it is even more difficult to hire outside consultants. With this paper, we present the theory for doing sophisticated mooring analysis, the hydrodynamic and material constants for typical buoy and mooring components, and examples that show engineers how to apply the concepts to their designs.

Beyond this, we tailor the analysis to the specific structure of an instrumented oceanographic mooring. Because of the small relative size of the buoy, interaction between the mooring cable and the buoy must be taken into account. For large moored offshore structures, cable-structure interactions can be simplified by using a quasi-static approach which assumes that the dynamics of the cable do not effect the motion of the buoy.

In the next section, we review procedures for calculating the static configuration of the mooring and present numerical and analytical tools for predicting dynamic loads. This includes a presentation of methods for calculating hydrodynamic coefficients of small axisymmetric buoys which are needed for the dynamic calculations. Sample calculations are presented that show that the dynamic tensions in the mooring line are controlled primarily by the heave motion of the buoy and the longitudinal motion of the mooring. We use this result in Section 3 to construct a simple analyt-

ical model for predicting dynamic tensions in surface moorings that gives comparable results to the numerical method and matches full-scale experimental data. In Section 4, we show how to combine results from static and dynamic analysis to predict ultimate failures and fatigue failures. A design example is given in Section 5 followed by conclusions.

STATIC AND DYNAMIC CALCULATIONS

The numerical calculations for the statics and dynamics, which we present in this section, are based on the equations of motion of the cable, attached instruments, and the surface buoy. We assume that all the motion is confined to a single plane so that a two-dimensional formulation applies. For the dynamics, we linearize motion about the nonlinear static configuration and perform frequency domain calculations. Our mathematical formulation follows the procedures described in Goodman *et al.* (1972). The numerical calculations for the statics are identical to Goodman *et al.* (1972) while the dynamics are modified to include nonlinear drag effects through an equivalent linearization procedure (Triantafyllou *et al.*, 1987). We also present a novel scheme that reduces the solution to a simple closed form matrix equation.

Static Calculations

We start with the equations for the static equilibrium of a cable element of unstretched length ds, weight in water per unit unstretched length w_o, stretched cross-sectional area A, and Young's modulus E. Using the derivation and nomenclature given in Triantafyllou *et al.* (1987) we can write:

$$\frac{\partial T_o}{\partial s} = w_o \sin\phi_o - F_{to}(1+e_o) \tag{1}$$

$$\frac{\partial \phi_o}{\partial s} = \frac{1}{T_o}\left[w_o \cos\phi_o + F_{no}(1+e_o)\right] \tag{2}$$

where T_o is the effective static tension (Goodman and Breslin, 1976), ϕ_o is the static equilibrium angle of the cable, and $e_o = T_o/EA$ is the static strain. The coordinate system is taken along the cable with position s and unit vectors $\hat{t}$ and $\hat{n}$ representing the tangential (along the axis of the cable) and normal (perpendicular to the axis of the cable) directions (Fig. 6). The fluid forces, resolved along the coordinate axis, are given in

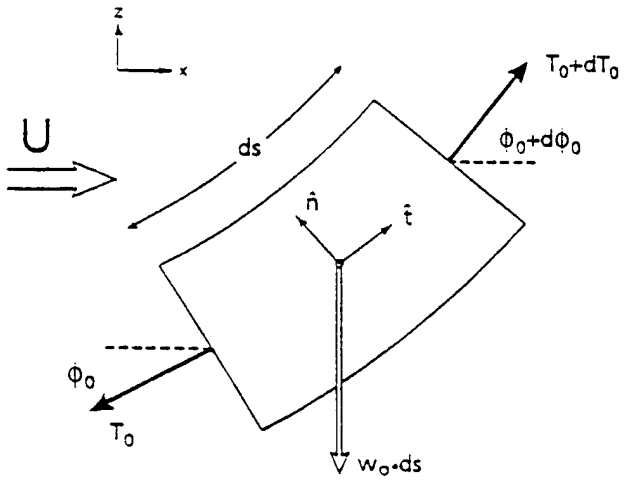

Figure 6: Cable coordinate system.

(Breslin, 1974). The fluid force tangential to the cable axis is:

$$F_{to}(1+e_o) = \frac{1}{2}\rho C_{Dt}\pi D_o U\cos\phi_o|U\cos\phi_o|\sqrt{1+e_o} \tag{3}$$

and the fluid force normal to the cable axis is:

$$F_{no}(1+e_o) = -\frac{1}{2}\rho C_{Dn} D_o U\cos\phi_o|U\cos\phi_o|\sqrt{1+e_o} \tag{4}$$

where D_o is the diameter of the unstretched cable, ρ is the density of water, and U is the current speed as a function of depth.

The frictional and normal drag coefficients are represented by C_{Dt} and C_{Dn} respectively. C_{Dt} is not important for static calculations since the moorings are, for the most part, nearly vertical and the current is assumed to be horizontal. A value of $C_{Dt} = 0.003$ is most often used based on calculations of local skin friction for steady turbulent flow along a long cylinder (White, 1974). The normal drag coefficient of a cable is influenced by vortex-induced vibrations and can range from a value of $C_{Dn} = 1.2$ for a nonvibrating, smooth circular cylinder to values greater than $C_{Dn} = 2.0$ for cables vibrating with amplitudes on the order of one cable diameter. Kim *et al.* (1986) measured drag coefficients of 1.4 to 1.6 for a long vertical cables that were lightly tensioned and hanging in a shear current. Grosenbaugh *et al.* (1991) measured

drag coefficients for long vertical tow cables that had similar tension to that of a mooring cable and found drag coefficients between 1.6 and 2.0 in shear currents. For the mooring calculations presented in this paper, we use a value of $C_{Dn} = 1.6$.

There are also two geometric relations that give the position of the cable in cartesian x, z-coordinates. These are:

$$\frac{\partial x_o}{\partial s} = (1 + e_o)\cos\phi_o \tag{5}$$

$$\frac{\partial z_o}{\partial s} = (1 + e_o)\sin\phi_o \tag{6}$$

The two cable equations and the two geometric relations along with appropriate boundary conditions can be integrated using Runge-Kutta methods (Forsythe *et al.*, 1977) to give effective static tension T_o, cable angle ϕ_o, and x, z-configuration. The integration begins at the surface buoy ($s = L$ where L is the total unstretched length of the composite mooring line) with boundary conditions:

$$\begin{aligned} T_o(L) &= F_{bo}\left[\cos\phi_o(L)\right]^{-1} \\ x_o(L) &= 0 \\ z_o(L) &= 0 \end{aligned} \tag{7}$$

F_{bo} is the steady fluid drag force acting on the buoy and is given by:

$$F_{bo} = \frac{1}{2}\rho C_{Db} A_b U_b |U_b| \tag{8}$$

where C_{Db} is the drag coefficient, A_b is the horizontal projected area of the buoy and U_b is the current speed at the surface buoy.

These boundary conditions assume that all the forces act through the center of gravity and that the change in the draft of the buoy due to the cable tension is small. More complicated boundary conditions that allow for the calculation of the equilibrium draft and pitch can be used. However we find them to be unnecessary because of the large waterplane area of the surface buoys used on oceanographic moorings and the large weight of attached instruments which helps keep the buoy nearly vertical. The final boundary condition is that the bottom of the mooring cable at $s = 0$ is located precisely at the anchor. This can be expressed mathematically as:

$$z_o(0) = -d \tag{9}$$

where d is the water depth.

The static solution is found by guessing the cable angle at the top of the mooring line, using the guess to calculate the other initial conditions from equation (7), and then integrating the cable equations to find T_o, ϕ_o, x_o, and z_o as a function of s. If equation (9) is satisfied, the calculated values represent the true solution. If the end of the cable is above or below the anchor, then the calculations must be repeated with a modified value of $\phi_o(L)$. The Newton-Raphson iteration process (Forsythe *et al.*, 1977) continues until the correct value of $\phi_o(L)$ is chosen, and the bottom boundary constraint is satisfied.

The attached instruments are treated as cable elements and assigned an equivalent weight in water per unit length, a diameter, and drag coefficients that give the proper forces. This is made necessary by the fact that some instrument cages are more than 2 meters long. The combined instrument string can represent 20 to 40 meters of the total length of the mooring line. An alternate (and equivalent) method (Goodman *et al.*, 1972) is to treat the instruments as point masses though the extra length of the instruments still needs to be taken into account.

In analyzing the statics of an oceanographic mooring, the standard procedure is to examine two different current cases. The first case, called the "survival current", represents an extreme current profile. Using this in the static calculations gives the maximum static load at each location of the mooring line. It also provides the input in terms of the equilibrium cable configuration and tension for dynamic calculations which are needed to predict total extreme loads. The second case, called the "design current" corresponds to typical operating conditions. The results of static calculations using this profile are used to verify that the angles of the instruments are within the design range ($< 15°$ from the vertical). The "design" configuration and tensions are also used as input for the numerical codes to predict the dynamic tensions that are used in the fatigue analysis.

Dynamic Calculations

The dynamics are calculated by linearizing the motion about the static configuration. We assume that all the dependent variables (i.e. the tension, the cable angle, the longitudinal and transverse motion, and the strain) are made up of a static part and a small dynamic part. As shown in reference (Triantafyllou *et al.*, 1987), the two-dimensional dynamic equations for a cable element of mass per unit unstretched length m_o,

longitudinal added mass per unit unstretched length m_{pa}, and transverse added mass per unit unstreteched length m_{qa} can then be written as:

$$(m_o + m_{pa})\frac{\partial^2 p}{\partial t^2} = \frac{\partial T_1}{\partial s} - T_o\frac{d\phi_o}{ds}\phi_1 + F_{t1} \qquad (10)$$

$$(m_o + m_{qa})\frac{\partial^2 q}{\partial t^2} = \frac{d\phi_o}{ds}T_1 + T_o\frac{\partial \phi_1}{\partial s} + \frac{dT_o}{ds}\phi_1 + F_{n1} \qquad (11)$$

$$\frac{\partial p}{\partial s} - d\phi_o dsq = T_1/EA \qquad (12)$$

$$\frac{\partial q}{\partial s} + d\phi_o dsp = \phi_1(1 + e_o) \qquad (13)$$

where p is the amplitude of longitudinal motion, q is the amplitude of transverse motion, T_1 is the dynamic tension, and ϕ_1 is the dynamic angle. The values of T_o and ϕ_o are known from the static solution. The total tension and angle are then given by:

$$T = T_o + T_1 \qquad (14)$$
$$\phi = \phi_o + \phi_1 \qquad (15)$$

The added mass in the longitudinal direction is zero for the mooring cable but has a significant value for the attached instruments.

The fluid forces are approximated by equivalent linear terms such that:

$$F_{t1} = -b_p\frac{\partial p}{\partial t} \qquad (16)$$
$$F_{n1} = -b_q\frac{\partial q}{\partial t} \qquad (17)$$

We determine the values of b_p and b_q by assuming harmonic motion and equating energy lost per cycle for the linear and nonlinear drag representations (Paulling, 1979). The expressions used in the calculations which take into account the magnitude of the steady current are (Triantafyllou *et al.*, 1987):

$$b_p = c_e\rho C_{Dt}\pi d\omega\,|\bar{p}| \qquad (18)$$
$$b_q = c_e\rho C_{Dn} d\omega\,|\bar{q}| \qquad (19)$$

where ω is the frequency of motion and $|\bar{p}|$ and $|\bar{q}|$ are the respective amplitudes of the longitudinal and transverse harmonic motion. The value of coefficient c_e depends on the current velocity and is given by:

$$c_e = \frac{2}{\pi}\left[\frac{(2 + U_R^2)\sqrt{1 - U_R^2}}{3} + U_R \arcsin U_R\right] \qquad (20)$$

where U_R is the absolute value of the ratio between the current velocity and the cable velocity either $|U/\omega p|$ or $|U/\omega q|$. For values of $U_R > 1$, $c_e = U_R$.

For a narrow banded random input such as that for irregular seas, the expression b_p and b_q become (Caughey, 1963):

$$b_p = c_e\rho C_{Dt}\pi d\sigma_{\dot{p}} \qquad (21)$$
$$b_q = c_e\rho C_{Dn} d\sigma_{\dot{q}} \qquad (22)$$

where $\sigma_{\dot{p}}$ is the standard deviation of the longitudinal cable velocity and $\sigma_{\dot{p}}$ the standard deviation of the transverse cable velocity. The coefficient c_e becomes:

$$c_e = \sqrt{\frac{2}{\pi}}e^{\frac{-U_R^2}{2}} + U_R erf\left(U_R/\sqrt{2}\right) \qquad (23)$$

where now $U_R = |U/\sigma_{\dot{p}}|$ or $U_R = |U/\sigma_{\dot{q}}|$ depending on the direction of motion. For both simple harmonic motion and irregular motion defined by an input spectrum, the damping constants b_p and b_q depend on the solution which must be obtained by iteration.

The solution in the frequency domain is found by assuming:

$$T_1 = \bar{T}_1 e^{i\omega t} \qquad (24)$$
$$\phi_1 = \bar{\phi}_1 e^{i\omega t} \qquad (25)$$
$$p = \bar{p}e^{i\omega t} \qquad (26)$$
$$q = \bar{q}e^{i\omega t} \qquad (27)$$

where $\bar{T}_1$, $\bar{\phi}_1$, $\bar{p}$, and $\bar{q}$ are complex amplitudes. The expressions are substituted into equations (10-13) to obtain ordinary differential equations with respect to the spatial variable s. We can write these in matrix form as:

$$\frac{d\vec{y}}{ds} = \mathrm{A}\vec{y} \qquad (28)$$

where $\vec{y}$ is defined as:

$$\vec{y} = \begin{pmatrix} \bar{T}_1 \\ \bar{\phi}_1 \\ \bar{p} \\ \bar{q} \end{pmatrix} \qquad (29)$$

M is the mass of the buoy, μ_{11}, μ_{33}, μ_{55}, and μ_{15} are frequency dependent added mass coefficients, λ_{11}, λ_{33}, λ_{55}, and λ_{15} are frequency dependent wave damping coefficients, C_{33} and C_{55} are the restoring constants for heave and pitch, and $F_{\eta 1}$, $F_{\eta 3}$, and $F_{\eta 5}$ are the wave forces and moments. In the next section, we describe how to calculate the hydrodynamic coefficients and wave forces for an axisymmetric buoy and give values for three different buoy shapes.

The equations of motion for the buoy are written about its center of gravity. Here, we allow the connection point between the cable and the buoy to be located at any height above or below the center of gravity. This distance is represented in equation (37) by z_c.

If we assume that the buoy motions are harmonic along with the tension and cable angle at the top of the mooring, then equations (35-37) simplify to:

$$\mathbf{H} \begin{pmatrix} \tilde{\xi}_1 \\ \tilde{\xi}_3 \\ \tilde{\xi}_5 \end{pmatrix} = \tilde{F}_\eta + \mathbf{G} \begin{pmatrix} \tilde{T}_N \\ \tilde{\phi}_N \end{pmatrix} \tag{38}$$

where H is a complex matrix containing the buoy mass plus hydrodynamic coefficients, $\tilde{F}_\eta$ is a complex vector which represents the wave forces, and G is complex matrix that is a function of the static tension and angle at the top of the cable.

The boundary condition at the top of the cable is that its motion is compatible with the motion of the buoy. They are related by:

$$\begin{pmatrix} \tilde{p}_N \\ \tilde{q}_N \end{pmatrix} = \mathbf{R} \begin{pmatrix} \tilde{\xi}_1 \\ \tilde{\xi}_3 \\ \tilde{\xi}_5 \end{pmatrix} \tag{39}$$

$$\mathbf{R} = \begin{pmatrix} \cos\phi_o & \sin\phi_o & -z_c\cos\phi_o \\ -\sin\phi_o & \cos\phi_o & z_c\sin\phi_o \end{pmatrix}$$

where R is a 2×3 matrix that relates the cable coordinate system to the buoy coordinated system. If we left multiply both sides of equation (38) by $\mathbf{RH}^{-1}$ and use equation (34) to eliminate $\tilde{T}_N$ and $\tilde{\phi}_N$, we finally arrive at an expression for the motion of the top of the mooring cable in terms of known input. The expression is:

$$\begin{pmatrix} \tilde{p}_N \\ \tilde{q}_N \end{pmatrix} = \left[\mathbf{I} - \mathbf{RH}^{-1}\mathbf{GB}_{11}\mathbf{B}_{21}^{-1}\right]^{-1} \mathbf{RH}^{-1}\tilde{F}_\eta \tag{40}$$

Once $\tilde{p}_N$ and $\tilde{q}_N$ are found, the dynamic tension and dynamic cable angle at the anchor can be found from:

$$\begin{pmatrix} \tilde{T}_1 \\ \tilde{\varphi}_1 \end{pmatrix} = \mathbf{B}_{21}^{-1} \begin{pmatrix} \tilde{p}_N \\ \tilde{q}_N \end{pmatrix} \tag{41}$$

and then the motion, dynamic tension, and dynamic angle at nth node of the cable can calculated from the partial matrix product:

$$\tilde{y}_n = \left(\prod_{i=1}^{n} \mathbf{B}_i \right) \tilde{y}_1 \tag{42}$$

The buoy motion is found by inverting equation (39).

For harmonic calculations (i.e. at a particular wave frequency and wave amplitude), we guess that the amplitude of motion at each node $\tilde{p}_i$ and $\tilde{q}_i$ is equal to the wave amplitude. We use this guess to determine the $\mathbf{B}_i$'s and the $\mathbf{B}_{ij}$'s. We then solve equation (40) for $\tilde{p}_N$ and $\tilde{q}_N$ and equation (41) for $\tilde{T}_1$ and $\tilde{\varphi}_1$. Equation (42) allows us to solve for the motion along the length of the mooring line which are then compared to the original guess. This process continues until the guess and solution converge within a user specified error. Away from the natural elastic frequencies of the mooring cable, the solution process converges quickly, usually in two iteration steps. Convergence is slower near natural frequencies of the system.

For spectral analysis where the input is defined by a wave spectrum $S_\eta(\omega)$, the standard deviation of the longitudinal and transverse cable velocities $\sigma_{\dot{p}}$ and $\sigma_{\dot{q}}$ are initially set equal to the standard deviation of the wave velocity. This is used to calculate the transfer functions $H_p(\omega, s)$ and $H_q(\omega, s)$ for the longitudinal and transverse mooring motions. The spectrum of the cable motions $S_p(\omega, s)$ and $S_q(\omega, s)$ are then found from:

$$S_p(\omega, s) = |H_p(\omega, s)|^2 S_\eta(\omega) \tag{43}$$

$$S_q(\omega, s) = |H_q(\omega, s)|^2 S_\eta(\omega) \tag{44}$$

New values of $\sigma_{\dot{p}}$ and $\sigma_{\dot{q}}$ are found by integrating the velocity spectra which are just ω^2 times the motion spectra. The calculations are then repeated until convergence is achieved. The spectrum of the tensions at any location can then be calculated from:

$$S_T(\omega, s) = |H_T(\omega, s)|^2 S_\eta(\omega) \tag{45}$$

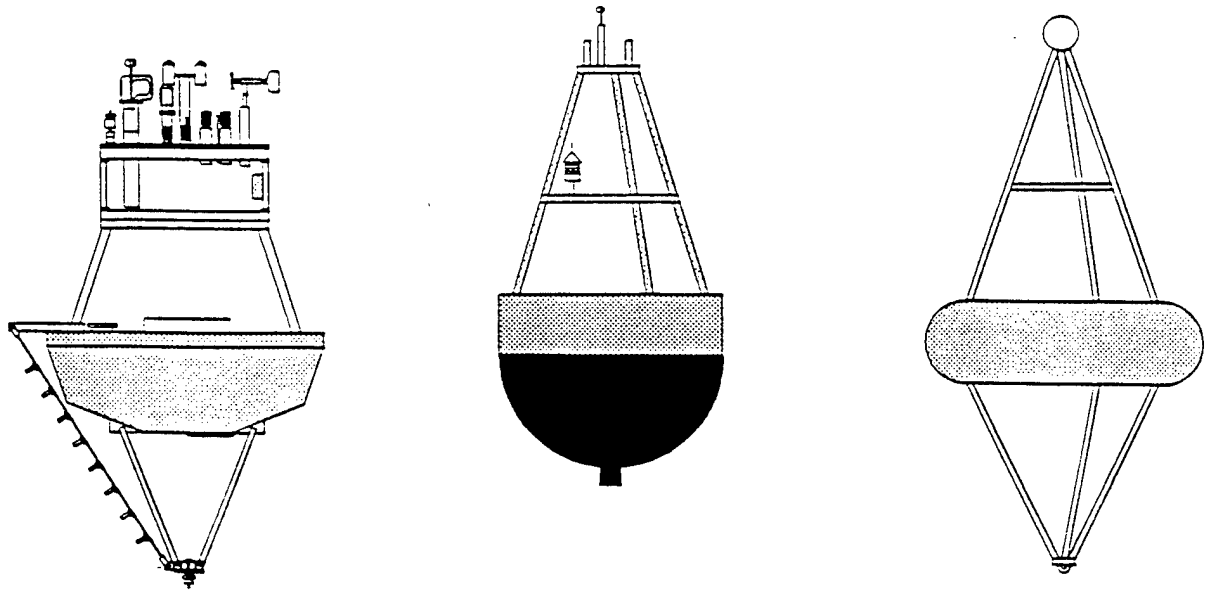

Discus Buoy		Spherical Buoy		Toroid Buoy	
Nominal Diameter	*3.0 m*	*Nominal Diameter*	*3.0 m*	*Nominal Diameter*	*2.4 m*
Waterplane Area	*6.2 m²*	*Waterplane Area*	*5.7 m²*	*Waterplane Area*	*4.0 m²*
Displaced Volume	*2.1 m³*	*Displaced Volume*	*3.8 m³*	*Displaced Volume*	*1.2 m³*
Metacentric Height	*1.1 m*	*Metacentric Height*	*0.37 m*	*Metacentric Height*	*1.1 m*
Moment of Inertia	*1900 kg-m²*	*Moment of Inertia*	*5200 kg-m²*	*Moment of Inertia*	*1400 kg-m²*

Figure 8: Typical oceanographic surface buoys.

Hydrodynamic Coefficients of Oceanographic Buoys

The two-dimensional numerical method just presented incorporates the exciting wave forces, moments, and hydrodynamic coefficients of the surface buoy into the calculations. Here we present the wave forces and moments and hydrodynamic coefficients for three oceanographic buoys that are currently being used on surface moorings (Fig. 8). The *8-foot toroid buoy* was used on the original oceanographic surface moorings of the 1960's, and is still used today on ATLAS moorings (Milburn and McClain, 1986). The *3-meter discus buoy* was developed in the late 1970's to fill the need of increased payload and reserve buoyancy (Berteaux and Roy, 1986). It has become the workhorse of the oceanographic community. The *10-foot spherical buoy* was developed recently as a buoy with large reserve buoyancy and a shape that has improved seakeeping qualities. To date, it has been used exclusively on oceanographic engineering test moorings. Buoy characteristics are listed in Table 1.

All of the buoys in Fig. 8 are axisymmetric about the vertical axis. This fact is used to simplify the calculations. We consider a free floating vertical axisymmetric body excited by regular waves of amplitude η and frequency ω propagating in water depth d. Cylindrical coordinates (r,θ,z) are introduced with origin at the undisturbed water surface and the z-axis positive upwards. Viscous effects are neglected and the assumption is made that the fluid is incompressible. The motions of the body and the fluid are assumed to be small so that linear potential theory can be applied to describe the fluid motion. The flow is governed by the velocity potential Φ which satisfies the Laplace equation within the fluid domain and the appropriate boundary conditions on the free surface, the sea bottom, the wetted surface of the body, and the radiation condition at infinity (Mei, 1983).

We examine the in-plane motion (surge ξ_1, heave ξ_3, and pitch ξ_5) of the buoy in regular waves. The velocity potential for this case can be expressed as:

$$\Phi(r,\theta,z,t) = Re\left\{\phi(r,\theta,z)e^{-i\omega t}\right\} \qquad (45)$$

with

$$\phi(r,\theta,z) = \phi_0(r,\theta,z) + \phi_7(r,\theta,z) + \sum_{j=1,3,5} \xi_j \phi(r,\theta,z) \tag{46}$$

Here, ϕ_0 is the velocity potential of the undisturbed incident harmonic wave, ϕ_7 is the diffraction potential for the body fixed in the wave, and ϕ_j is the radiation potential resulting from the forced body motion in the jth mode of motion with unit velocity amplitude ξ_j.

The velocity potential of the undisturbed incident wave can be expressed in cylindrical coordinates as:

$$\phi_0(r,\theta,z) = \tag{47}$$
$$-i\omega\eta \frac{\cosh[k(z+d)]}{k \sinh kd} \sum_{m=0}^{\infty} \epsilon_m i^m J_m(kr) \cos m\theta$$

where J_m is the mth order Bessel function of first kind and ϵ_m is the Neumann's symbol such that $\epsilon_0 = 1$ and $\epsilon_m = 2$ for $m \geq 1$. The frequency ω and wave number k are related by the dispersion relation:

$$\omega^2 = gk \tanh kd \tag{48}$$

In a similar manner, the diffraction and radiation potentials can be written in the form:

$$\phi_j(r,\theta,z) = -i\omega\eta \sum_{m=0}^{\infty} \epsilon_m i^m \Psi_{jm}(r,z) \cos m\theta \tag{49}$$

for $j = 1, 3, 5, 7$. In this case, the unknown complex functions Ψ_{jm} are established through the method of matched axisymmetric eigenfunction expansions. This method was introduced in (Garrett, 1971) for the solution of the diffraction problem around a vertical cylinder and used for both the diffraction and radiation problem of a vertical cylinder in (Yeung, 1981). The technique that we use for calculating the wave exciting forces and hydrodynamic coefficients is an extension to arbitrarily shaped vertical axisymmetric bodies that is described in (Mavrakos, 1985; Kokkinowrachos *et al.*, 1986; Mavrakos, 1988).

Given the solutions for the velocity potentials ϕ_7 and ϕ_j, we can determine the exciting wave forces and moments used in equations (35-37) from:

$$F_{ej} = -i\omega\rho \int\int (\phi_0 + \phi_7)\, n_j\, dS \tag{50}$$

where the integration is taken over the wetted surface area of the buoy. Here, n_j is defined in terms of the unit normal vector $\hat{n}$ and position vector $\vec{r}$ such that:

$$(n_1, n_2, n_3) = \hat{n} \qquad (n_4, n_5, n_6) = \vec{r} \times \hat{n} \tag{51}$$

where we are interested in the planer components n_1, n_3, and n_5. The hydrodynamic added mass μ_{ij} and damping λ_{ij} are given by:

$$\mu_{ij} + \frac{i}{\omega}\lambda_{ij} = -\rho \int\int \phi_j \mathrm{n}_i dS \tag{52}$$

The method outlined above has been used to obtain the hydrodynamic characteristics of the three oceanographic buoys depicted in Fig. 8. The exciting forces, moments, and hydrodynamic coefficients for surge, heave, and pitch are given in Figs. 9-11. The curves correspond to $d = 100$ m, though the results are nearly identical to those found for $d = \infty$.

As can be seen from Fig. 9, where the toroidal oceanographic buoy is considered, a peculiar behavior of both the heave exciting forces and the hydrodynamic parameters is obtained near $f = 0.7$ Hz. This behavior, which is typical of toroidal bodies (Garrett, 1970; Newman, 1977; Miloh, 1983), arises from the resonance heave oscillation of the free surface enclosed by the toroid. In the neighborhood of this resonance, negative values of the added mass coefficients are obtained though the damping coefficients always remain positive.

Sample Calculations of Surface Moorings

Sample calculations are presented to show the dynamic characteristics of oceanographic surface moorings. We will use the design for the 1991 MLML mooring. This mooring was an inverse-catenary mooring deployed in 2850 m of water. In order to examine characteristics of taut moorings, we perform some of the calculations using a depth of 3700 m which is equal to the total length of the mooring line (Fig. 12).

The mooring consisted of a 90 m long instrument string followed by 500 m of 7/16-inch and 1710 m of 3/8-inch diameter wire rope, 680 m of 7/8-inch diameter nylon rope, 690 m of 1-1/8-inch diameter polypropylene rope, and 130 m of glass-balls mounted on chain along with the anchor tackle. The instrument string had five Multi-Variable Moored Systems (MVMS) which are modified VMCMs with additional sensors mounted in the cage, four bio-optical sensors (BOMS) which, like a SEACAT, these consist of an instrument pressure housing that is mounted on a steel rod, one ADCP, one engineering instrument that is attached in-line to measure mooring-line

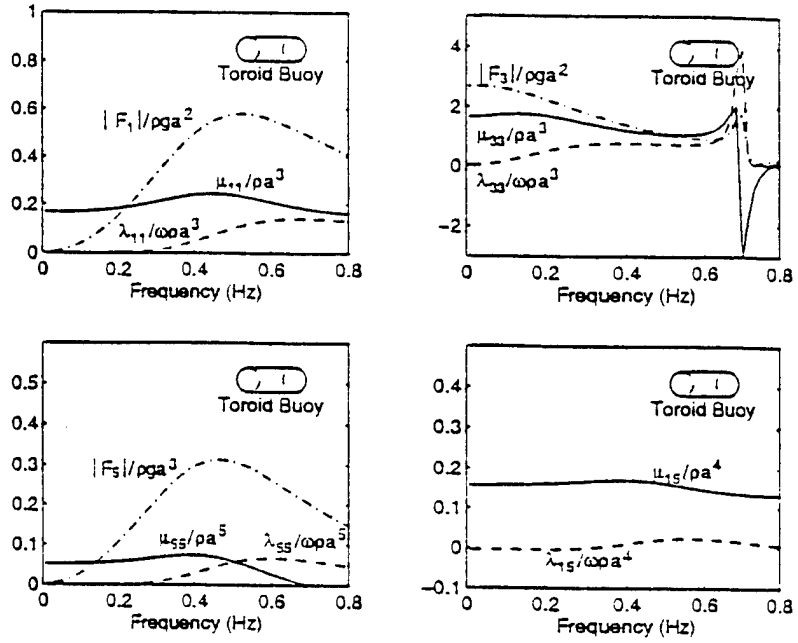

Figure 9: Hydrodynamic coefficients, wave forces, and wave moments for toroid buoy.

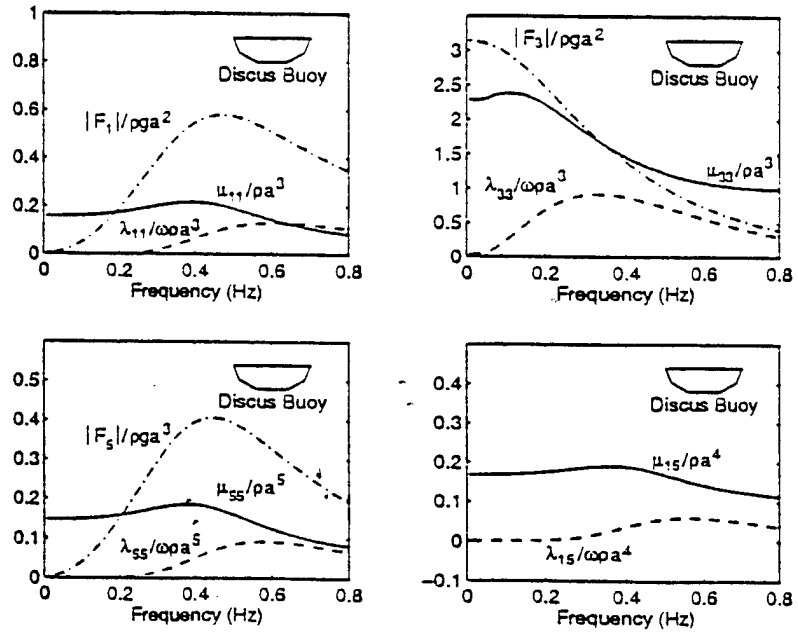

Figure 10: Hydrodynamic coefficients, wave forces, and wave moments for discus buoy.

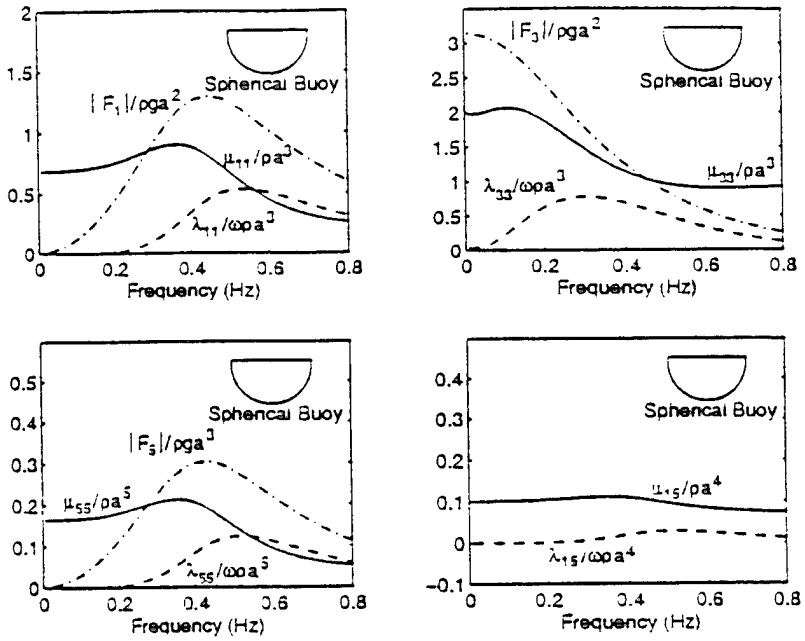

Figure 11: Hydrodynamic coefficients, wave forces, and wave moments for spherical buoy.

tension, and one custom-made bioluminescence sensor (MOORDEX). Important characteristics of the instruments are given in the Appendix.

The static configurations are calculated as described at the beginning of this section, and these are used as input for the dynamic calculations. We use a uniform (with depth) current of 0.02 m/s for slack conditions. For moderate currents (i.e. design current), we use a profile that is equal to 0.60 m/s from the surface down to a depth of 100 m, decreasing linearly to 0.25 m/s at 1500 m depth, and then decreasing to 0.05 m/s at the anchor. The biggest difference between the taut mooring and the inverse-catenary mooring is the static tension in moderate currents (Fig. 12). The larger tensions in the taut mooring (30,400 N for the taut mooring versus 17,700 N for the inverse catenary in moderate currents) increase the chances of the mooring components breaking, the buoy being pulled underwater, or having its anchor drag.

For the initial dynamic calculation, we determine the transfer function of the dynamic tension at the top of the taut mooring with a *3-meter discus buoy* in Sea States 3 and 7. We use the static configuration corresponding to the taut mooring in moderate currents. The key features of the transfer functions (Fig. 13) are the low frequency behavior corresponding to the acceleration of the mass of the instruments and wire rope (plus the drag of the instruments in high sea states), the fundamental elastic natural frequency of the nylon rope near 0.3 Hz and the heave natural frequency of the buoy near 0.4 Hz. These natural frequencies are more damped in the higher sea states. The dynamic coefficient of friction for the wire rope and synthetic rope is taken as $C_f = 0.003$ (Grosenbaugh, 1995a).

Additional resonant frequencies above 0.5 Hz are present but are relatively unimportant because of the limited wave energy at these frequencies. This can be seen in plots of the motion spectra of the buoy for surge, heave, and, pitch (Fig. 14) where, for the most part, the buoy follows waves. The pitch calculations are based on potential flow, and the real response most likely has more damping which would lower the resonant response.

We recalculate the transfer functions of the dynamic tension using the the *8-foot toroid buoy* and *10-foot spherical buoy* and compare the results of all three buoys in Fig. 15. The discus and spherical

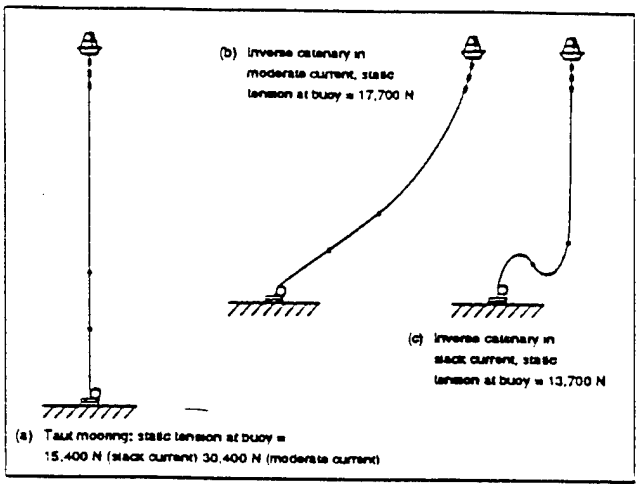

Figure 12: Static configurations for the three cases used in the numerical simulations. The parameters for the 1991 MLML mooring are use for each calculation.

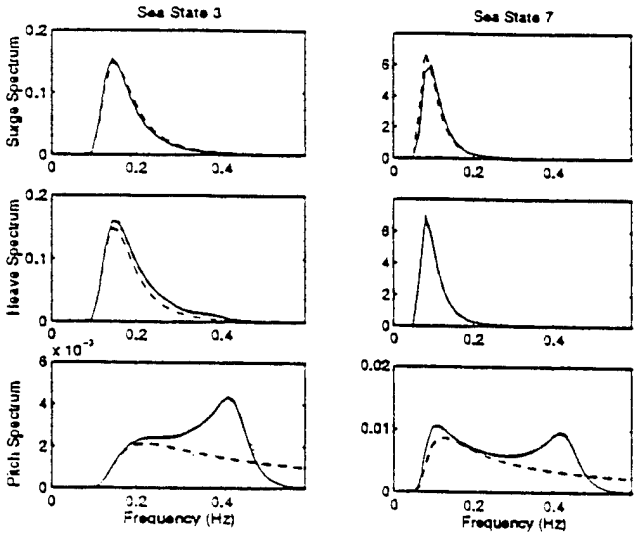

Figure 14: Power spectra of surge, heave, and pitch for a taut mooring with a discus buoy in Sea State 3 and Sea State 7.

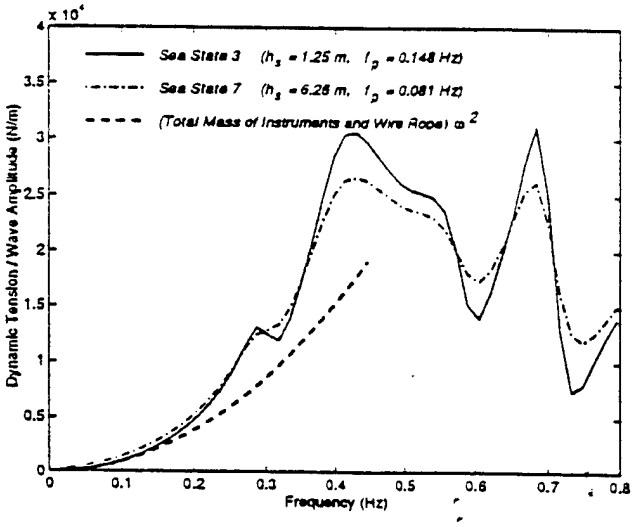

Figure 13: Transfer function of the tension at the top of a taut mooring with a discus buoy in Sea State 3 and Sea State 7.

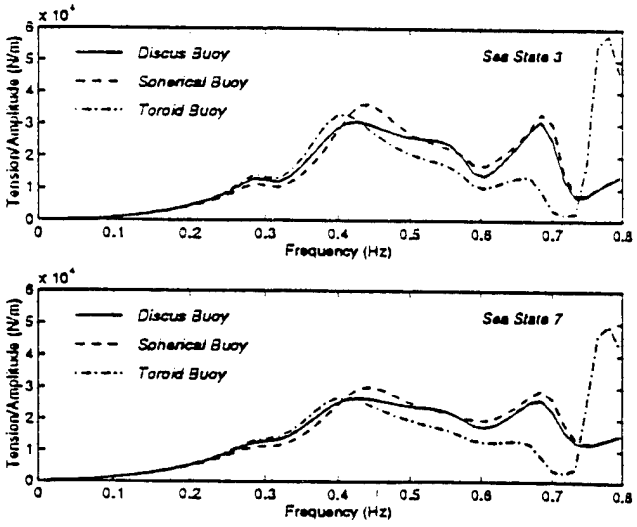

Figure 15: Comparison of transfer functions of the tension at the top of a taut mooring with three different buoy shapes.

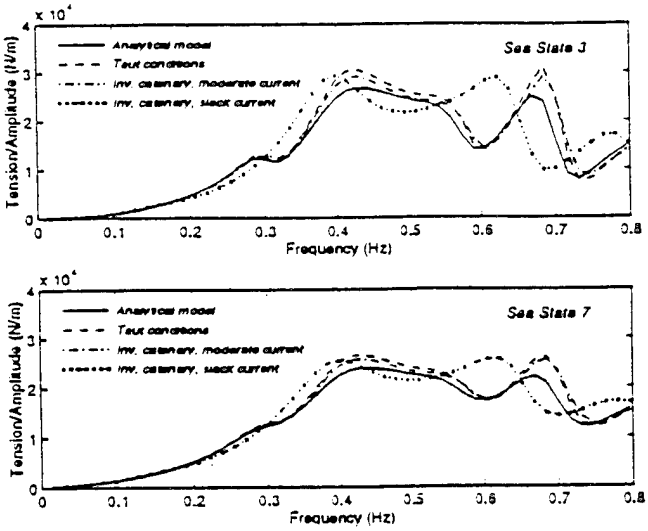

Figure 16: Comparison of transfer functions of the tension at the top of a taut mooring and an inverse-catenary mooring in moderate and slack current conditions. The analytical model represented by the solid curve is described in Section 3.

Sea State	Discus	Sphere	Toroid
3	2220 N	2150 N	2350 N
7	4130 N	3950 N	4250 N

Table 1: Comparison of the standard deviations of the tensions at the top of taut mooring for different buoy shapes.

buoys show little difference except for slight offset of the buoy natural frequency. The toroid buoy is similar at low frequencies but shows large differences near 0.75 Hz where the free-surface resonance within the center of the toroid occurs. The tensions on the mooring line calculated from Equation (45) show differences in Sea State 3 and in Sea State 7 with the spherical buoy giving the best result (Table 1).

The next calculation compares the dynamic tensions of a taut mooring and an inverse-catenary moorings in slack and moderate current conditions. Each mooring uses a 3-meter discus buoy. In a weak current, the loop in the synthetic rope of the inverse-catenary mooring is present. In a moderate current, the loop is pulled nearly straight, and the total mooring line forms a catenary with positive curvature.

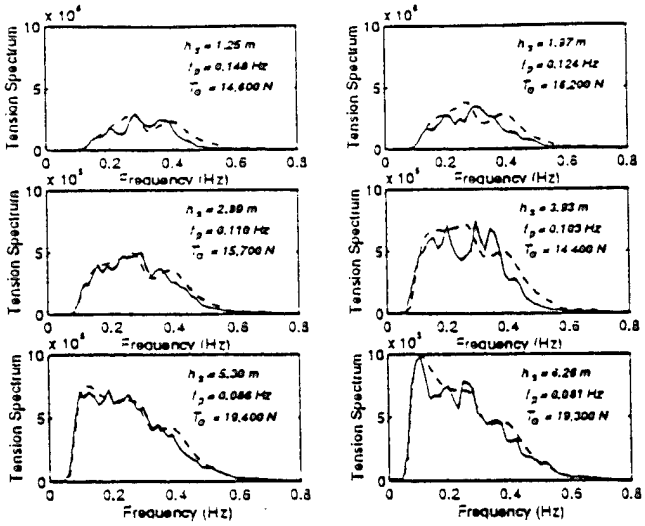

Figure 17: Comparison between measured tension power spectra for the 1991 MLML mooring and predictions based on numerical simulation.

The dynamic-tension transfer function of the moorings show that the response of the taut and inverse-catenary moorings in moderate currents are similar (Fig. 16). In slack current conditions the effects of the spring in the synthetic rope are absent so that the resonance at 0.3 Hz is not present and the heave natural frequency of the buoy is reduced. The solid curve corresponds to an analytical model that is described in the next section.

For the final calculation in this section, we use the inverse-catenary design of the 1991 MLML mooring and compare estimated tension spectra for six dif-

Sea State	Measured	Simulation	Analytical Model
3	1960 N	2160 N	2210 N
4	2340 N	2520 N	2570 N
5	2940 N	3010 N	3060 N
5+	3530 N	3690 N	3810 N
6	3750 N	3720 N	3780 N
7	4020 N	4050 N	4120 N

Table 2: Comparison of the standard deviations of the tensions at the top of 1991 MLML moorings for given sea states.

ferent sea states with actual measurements (Fig. 17). Qualitatively, the fit to the data is good. The standard deviation of the tensions, given in Table 2, show errors of 11% for the lowest sea state and errors that are less than 3% for the other sea states.

ANALYTICAL MODEL

In this section, we present an analytical model that can used for preliminary dynamic analysis of instrumented oceanographic surface moorings. The model simplifies the problem by treating only the vertical motion of the buoy and the longitudinal motion of the mooring line and attached instruments. We will show through comparison with the two-dimensional numerical model that the analytical model captures all the important dynamic effects and gives accurate predictions of the dynamic tension at the top of the mooring line.

The analytical model was proposed by Grosenbaugh (1995b) for predicting the tensions at the top of a mooring line where the tensions are greatest. The model simplifies the problem by treating only the vertical motion of the buoy and the longitudinal motion of the mooring line and attached instruments. The justification for this assumption is based on the effects of hydrodynamic damping. The transverse motions that are excited at the top by the buoy's surge and pitch motions dissipate quickly as they travel down the mooring line and have little effect on the dynamic tension. Conversely, the longitudinal motions are maintained by the hydrodynamic damping all the way down the mooring line even for the inverse-catenary mooring where the slope of the mooring line can become negative in slack current conditions.

The major simplifying assumption of the model is that the dynamics of the instruments and their connecting hardware can be combined into a single point mass and damper that hangs just below the buoy. The instruments are typically located within the top few hundred meters of the mooring. Our assumption is that the whole instrument string moves as a single unit with the same amplitude and phase of the surface buoy. This creates an effect where the dynamic tension at top of the mooring line is a function of the sum of their mass, added mass, and viscous damping. In fact, for a heavily instrumented mooring, 90-95% of the dynamic tension can be attributed to the instruments. The remaining tension comes from the elastic strain of the wire and synthetic rope.

Using these assumptions, the system is represented by three coupled differential equations: one describing the heave motion of the buoy, one describing the vertical motion of the instruments (i.e. point mass and damper), and one describing the longitudinal motion of the combination wire rope/synthetic rope mooring line. These can be solved to give the transfer function of the tension at the top of the mooring. The spectral response for a given sea state can then be calculated from equation (45). For a string of instruments with total mass and added mass of $\mathcal{M}$ including any hardware used to connect the instruments together and an equivalent linearized damping constant $\mathcal{B}$ which is related to the number and size of the instruments, the transfer function of the tension is:

$$H_T(\omega) = H_Z(\omega)\left[-\mathcal{M}\omega^2 + i\mathcal{B}\omega + \alpha(E_s A_s k_s \cot k_s L_s - E_w A_w k_w \tan k_w L_w)\right] \tag{54}$$

The first two terms in brackets account for inertia and drag of the instrument string located above the wire rope. The drag force on the instruments is a function of the standard deviation of the buoy's heave velocity which is calculated from the buoy's heave transfer function as described below. The third term in brackets is associated with the strain of the synthetic rope where E_s is Young's modulus, A_s is the cross-sectional area, and L_s is the length of the synthetic rope. This term becomes important when $k_s L_s = \pi/2$ which defines the fundamental elastic natural frequency. The wave number of the synthetic rope k_s is defined by:

$$k_s = \left(\frac{m_s\omega^2 - i\sigma_{\dot{p}} b_s \omega}{E_s A_s}\right)^{\frac{1}{2}} \tag{55}$$

where $\sigma_{\dot{p}}$ is the standard deviation of the mooring line's longitudinal velocity averaged over the length of the synthetic rope, m_s is the mass per unit length, and b_s is the equivalent linearized damping constant per unit length of the synthetic rope. The last term in brackets is associated with the response of the wire rope where E_w is Young's modulus, A_w is the cross-sectional area, and L_w is the length of the wire rope. The wave number k_w is given by:

$$k_w = \left(\frac{m_w\omega^2 - i\sigma_{\dot{p}} b_w \omega}{E_w A_w}\right)^{\frac{1}{2}} \tag{56}$$

where m_w is the mass per unit length and b_w is the equivalent linearized damping constant per unit length

of the wire rope. Again, σ_p is averaged over the length of the wire rope.

Finally, the term $H_Z(\omega)$ is the transfer function of the buoy's heave response in waves taking into account the presence of the instruments and the mooring line. It is given by:

$$H_Z(\omega) = F_{\eta z}\left[C_{33} - M_\Sigma\omega^2 + iB_\Sigma\omega + \alpha(E_s A_s k_s \cot k_s L_s - E_w A_w k_w \tan k_w L_w)\right]^{-1} \quad (57)$$

where $M_\Sigma = M + M_{33} + \mathcal{M} + \mathcal{M}_a$ is the sum of the mass and added mass of the buoy and the instrument string, $B_\Sigma = B_{33} + \mathcal{B}$ is the sum of the damping of the buoy and the instrument string, and

$$\alpha = \left(1 + \frac{E_s A_s k_s}{E_w A_w k_w}\cot k_s L_s \tan k_w L_w\right)^{-1} \quad (58)$$

The heave motion of the buoy for a given sea state is given by:

$$S_Z(\omega) = |H_U(\omega)|^2 S_\eta(\omega) \quad (59)$$

where $S_Z(\omega)$ is the power spectrum of the buoy motion. Integration of ω^2 times the motion spectrum gives standard deviation of the heave velocity which is used to calculate the damping coefficient of the instruments.

The analytical model is compared in Fig. 16 to the three different configurations of the 1991 MLML inverse catenary mooring shown in Fig. 12. The comparison between the analytical model and the numerical model is made using the transfer function of the dynamic tension $H_T(\omega)$ given by Equation (55) and the parameters listed in Table 3.

For both small and large sea states, the analytical model gives similar results to those of the numerical model of the taut mooring and the inverse-catenary mooring in moderate currents. For the 1991 MLML mooring, the configuration of the mooring line could be represented by the moderate-current case over 95% of the time. The spectra in Fig. 17 all correspond to moderate to strong currents, and the analytical model gives excellent fits to the full-scale measurements (Grosenbaugh, 1995b). The standard deviations of the tension for the six different sea states are nearly identical to the results of the numerical model (Table 2). This shows the validity of the assumption that the heave motion of the buoy and the longitudinal motion of the mooring line are the cause of the dynamic tension.

An advantage of the analytical model is that it shows explicitly the individual effects of the instruments, mooring hardware, wire rope and synthetic rope that go into the overall dynamic response. This is important to engineers in the early phases of the design process when it is being decided how many instruments and how much wire and synthetic rope will be used in the mooring. The analytical model is an order of magnitude faster than numerical simulations and gives accurate results for moorings with the instruments concentrated in the top 300 m of the mooring (Grosenbaugh, 1995b). At a minimum, the analytical model can be used to verify the results of numerical simulations.

Instrument String	Total mass ($\mathcal{M}$)	1080 kg
	Total added mass ($\mathcal{M}_a$)	400 kg
	Damping constant ($\mathcal{B}$)	1260 $N\,s^2/m^2$
	Length	90 m
Wire Rope	Mass per length (m_w)	0.45 $kg\,m^{-1}$
	Young's modulus (E_w)	1.0×10^{11} N/m^2
	Cross-sectional area (A_w)	1.2×10^{-4} m^2
	Length (L_w)	2110 m
	Friction coefficient (C_f)	0.003
Synthetic Rope	Mass per length (m_s)	0.33 $kg\,m^{-1}$
	Young's modulus (E_s)	4.8×10^8 N/m^2
	Cross-sectional area (A_s)	5.0×10^{-4} m^2
	Length (L_s)	1370 m
	Friction Coefficient (C_f)	0.003

Table 3: Parameters used in analytical model for 1991 MLML mooring.

ULTIMATE AND FATIGUE ANALYSIS

The flow chart shown in Fig. 5 serves as a guide in performing ultimate and fatigue failure analysis of a mooring. The first step in both processes involves characterizing the environmental forcing in terms of the expected currents and waves. These are used to calculate static and dynamic tensions which are then incorporated into the failure analysis. The static and dynamic results are then combined during the ultimate failure analysis. The fatigue failure analysis is depends primarily on the dynamic results.

Design and survival current profiles are determined from historical oceanographic data. Many times the moorings are placed in locations that have never been instrumented and so estimates must be made.

Sea State No.	Wind Speed ($m\ s^{-1}$)	Significant Wave Height (m)	Peak Freq. (Hz)	Percentage Probability of Sea State
1	0-3.5	0.72	0.204	20.7
2	3.5-5.5	1.52	0.149	11.7
3	5.5-8.5	1.93	0.135	10.5
4	8.5-11	2.37	0.125	12.8
5	11-14	3.05	0.112	17.5
6	14-17	4.20	0.099	16.4
7	17-20	5.82	0.087	7.8
8	20-24	7.20	0.080	2.2
9	>24	9.00	0.074	0.4

Table 4: Sea state occurrences for Arabian Sea mooring site.

The current profiles used in the design of the Arabian Sea surface mooring were determined from ship observations of surface currents and estimates of how they changed with depth.

A description of the wave environment is constructed from observations within or near the deployment area. A source of such data is the *U.S. Navy Marine Climatic Atlas of the World* (Meserve, 1974) which can be used to construct a listing of the significant wave height, peak wave frequency, and probability of occurrence for a range of sea states. Wave data for the Arabian Sea surface mooring site are presented in Table 4. A wave amplitude spectrum corresponding to each sea state can be constructed by assuming that the shape is given by a modified Pierson-Moskowitz spectrum for fully-developed seas or a JONSWAP spectrum for fetch limited seas (Faltisen, 1990).

The next step is to calculate the static tension and equilibrium mooring configuration corresponding to the design and survival current profiles. The configuration is then used to determine the tension power spectrum for each sea state of interest. This can be done by calculating the transfer function of the tension numerically and using Equation (45) to determine $S_T(\omega)$. Alternatively, the analytical model can be used, if applicable, to calculate $H_T(\omega)$ at the top of the mooring where the tensions are the greatest, and this can be used for the components of the instrument string.

The standard deviation of the tension σ_T is needed for both the ultimate and fatigue failure analysis. This is determined from the tension spectra by

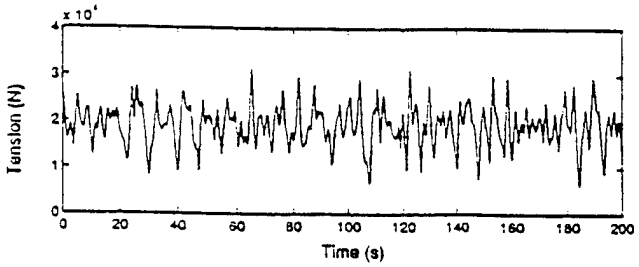

Figure 18: Time series of the tension at the top of the 1991 MLML mooring in Sea State 7.

computing:

$$\sigma_T = \left(\int_0^\infty S_T(\omega) d\omega \right)^{\frac{1}{2}} \tag{60}$$

In addition for fatigue failure analysis, the mean frequency (in Hertz) of the tension f_m for each sea state is needed and is determined from:

$$f_m = \frac{1}{2\pi\sigma_T} \left(\int_0^\infty \omega^2 S_T(\omega) d\omega \right)^{\frac{1}{2}} \tag{61}$$

Ultimate Failure Analysis

Ultimate failure analysis involves determining the maximum expected load on a mooring component and comparing this value to the ultimate strength. If the extreme load is greater than the ultimate strength then the part is likely to fail. In practice for oceanographic moorings, a safety factor of 2.5 is applied so that the design criterion for all mooring components is:

$$T_{extreme} < \frac{T_{ultimate}}{2.5} \tag{62}$$

The instantaneous tension on any mooring component is the combination of the static tension T_o and the dynamic tension T_1 as given by Equation (14). For oceanographic moorings that are heavely instrumented, the dynamic tension can be of the same magnitude as the static tension (Fig. 18) and, thus, cannot be ignored in calculating the total extreme load.

The static component of the extreme tension T_o^e is found using the survival current profile. The contribution from the dynamic tension is determined by first calculating σ_T using the survival current profile for the equilibrium mooring-line configuration and

the amplitude spectrum of the largest expected sea state. The extreme dynamic tension is then based on choosing the average tension of the highest $1/n$ tension amplitudes. We write this value as $T^{1/n}$ where we choose $n = 1000$. For the largest sea state in Table 5 (Sea State 7) which occurs 0.1% of the time over an eight month deployment, $T^{1/1000}$ turns out to be the average of the five highest dynamic tensions assuming a mean wave frequency of 0.25 Hz.

Water wave amplitudes closely follow a Rayleigh distribution. If we assume that the amplitudes of the tension also follow a Rayleigh distribution, we can write the extreme dynamic tension as:

$$T^{1/1000} = 3.85\sigma_T^s \tag{63}$$

where again σ_T^s is calculated from the survival current and the largest expected sea state. The extreme tension is then:

$$T_{extreme} = T_o^s + 3.85\sigma_T^s \tag{64}$$

This formula assumes the survival current occurs at the same time as the maximum dynamic tension, and thus provides additional margin of safety in the calculation.

Fatigue Failure Analysis

To predict the fatigue life of a mooring component, we adopt the *Palmgren-Miner* theory for cumulative damage (Miner, 1945). The theory is linear and assumes that fatigue damage occurring from a single cycle of loading at one amplitude can be added to the sum of the damage from all previous cycles even if the previous amplitudes were different. If a mooring component will break after a total of N cycles when subjected to a constant amplitude dynamic tension T, then it follows from the Palmgren-Miner theory that the fraction of damage after one cycle is N^{-1}.

If the same part is subjected to a narrow-banded random loading such as that caused by wave-induced motions during a particular sea state, then the fraction of damage over one cycle is the expected value of N^{-1}. If we assume again that the peak tensions follow a Rayleigh probability distribution, then it is easy to show (Triantafyllou *et al.*, 1986) that the expected value of N^{-1} corresponding to a given sea state is

$$E(N^{-1}) = \left(\frac{\sqrt{2}\sigma_T}{y}\right)^q \Gamma(1+\frac{q}{2}) \tag{65}$$

where Γ is a gamma function and σ_T is the standard deviation of the tension corresponding to a particular sea state. The parameters q and y are fatigue constants related to the material and geometry of the given mooring component.

The material constants are found from laboratory experiments in which a number of identical mooring components are cycled with constant-amplitude dynamic tension until they fail. The number of cycles at which the failure occurs is assumed to be related to the amplitude of the dynamic tension through:

$$N = \left(\frac{y}{T}\right)^q \tag{66}$$

Equation (66) is used widely to approximate components made of metal including wire rope. Synthetic rope can also be approximated with this equation but with a lesser degree of accuracy. By performing tests with different values of T, we can determine q and y using least-squares techniques.

We determined material constants for various sizes of galvanized-steel sling links and shackles like the ones used on the MLML moorings by choosing 12 parts and cycling them until one part failed. By doing this at different loads, we found that the links can be represented with $q = 3.8$ and $y = 1.7y_u$ (Fig. 19) and the shackles can be represented by $q = 3.7$ and $y = 1.5y_u$ (Fig. 20) where y_u is the ultimate strength of the given component. This method of taking the extreme minimum value was chosen because our emphasis is on insuring the survivability of the mooring.

We also tested the wire rope with swage fittings. This data is presented in Fig. 21 along with other wire-rope fatigue data from. Here the material constants are $q = 4.6$ and $y = 2.4y_u$.

The material values for the links and shackles correspond to tests performed at a mean tension of 17,800 N. To account for differences in the mean load, we determine an effective y and use this in Equation (65). The effective value y^* is given by (Collins, 1993):

$$y^* = y\left(\frac{y_u - 17,800}{y_u - T_m}\right) \tag{67}$$

where T_m is the mean tension which is determined from the static analyis.

The amount of fatigue damage due to a given sea state is the fraction of damage that occurs over one cycle times the total number of cycles that occur during that sea state. For a deployment that lasts a total of τ seconds, the number of cycles ν that occur

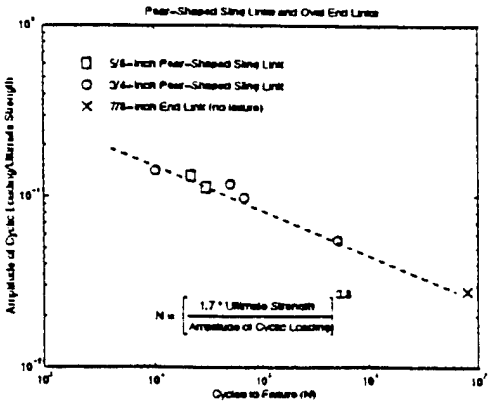

Figure 19: Cyclic fatigue curve for links.

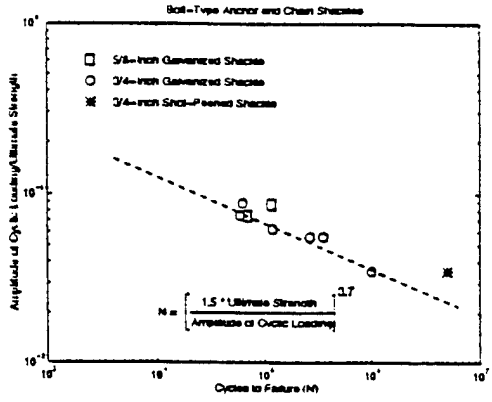

Figure 20: Cyclic fatigue curve for shackles.

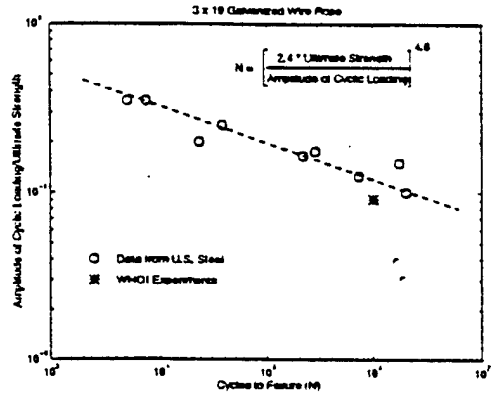

Figure 21: Cyclic fatigue curve for wire rope.

for a given sea state is:

$$\nu = \tau f_m P(h_s, f_p) \tag{68}$$

where $P(h_s, f_p)$ is the percentage probability of occurrence for a given sea state with significant wave height h_s and peak frequency f_p (Table 4). The fatigue damage for a given sea state is then:

$$D = \nu E(N^{-1}) \tag{69}$$

The total amount of fatigue damage for the whole deployment is the sum of the damage over all sea states. Thus, the criteria for predicting a fatigue failure is:

$$\sum_j D_j \geq \frac{1}{factor\ of\ safety} \tag{70}$$

where D_j is the damage associated with the jth sea state.

The factor of safety accounts for the uncertainties caused by the order of the loading and by the effects of corrosion. For quasi-random loading, the Miner's sum given by the left hand side of Equation (70) ranges between 0.6 and 1.6. Corrosion, on the other hand, can reduce fatigue strength by as much as half (Collins, 1993). Accordingly, we use a factor of safety of 4.0, accepting a mooring component only if the analysis shows that it loses no more than a quarter of its life during a deployment.

This analysis was applied in retrospect to the 1989 and 1991 MLML moorings (Grosenbaugh, 1995c). In particular, it predicted that the 5/8-inch pear-shaped sling link shown in Fig. 4 would last 44.4 days compared to the actual time to failure of 70 days. In addition, the 5/8-inch shackles used at the top of the mooring line would have had a fractional loss-of-life of 1.19. Based on our criteria of safety factor of four, this part would not have been acceptable. The fatigue resistance of the 1991 mooring was improved by using an inverse catenary design which helped to lower the mean tension, using 7/8-inch sling links and 3/4-inch shackles in the upper part of the mooring, and reducing the deployment time by 15%. The 7/8-inch sling links were predicted to have a fractional loss-of-life of 0.19 while the shackles were predicted to have a fractional loss of 0.23. The 1991 mooring was recovered with the mooring hardware showing little wear.

Design Example

We will analyze two components of the 1995 Arabian Sea Surface Mooring to demonstrate the design techniques for determining ultimate strength and

fatigue resistance. The components are a 3/4-inch chain shackle that is located at the top of the mooring where tensions are the highest and the 3/8-inch wire rope which begins at the bottom of the instrument string. The steps in this example are the same for all other mooring components so this can serve a step-by-step guide for engineering analysis.

The Arabian Sea surface mooring was an inverse-catenary mooring (Fig. 22) containing approximately 1150 m of 1 1/8-inch diameter polypropylene rope, 1680 m of 7/8-inch diameter nylon rope, and 1610 m of 3/8-inch and 7/16-inch diameter wire rope. Above this was a 250 m long instrument string containing 1/2-inch diameter wire rope, 3/4-inch chain, and a suite of instruments that included 5 VMCMs, four MVMSs, four SEACATs, one large custom made instrument for detecting zooplankton with sound (*Holiday Instrument*), and 13 temperature sensors.

The purpose of the mooring was to study ocean surface mixing in a region where cooling may occur during the summer. In the Arabian Sea, it is thought that strong monsoon winds during June, July, and August may cause increased mixing with the cooler water from below the surface. This hypothesis could only be answered with a surface mooring.

As seen in Table 4, the Arabian Sea is characterized by strong winds and high sea states. During 10% of the deployment, the winds are expected to be gale force. During the monsoon months this percentage increases to 25%. With the large number of instruments on the mooring, dynamic tensions will be high. Currents are also strong creating large static tensions.

The 3/4-inch shackles are used to attach all of the instruments to the mooring line, the most heavely tensioned shackle is located just above the top VMCM. Thus, for tensions in the analysis, we will use the tension at the top of the mooring line for the calculations. Fig. 23 shows the mooring configuration and static tension at the buoy in the design and survival currents. These were calculated using the static analysis procedures outlined in Section 2.

The dynamic tensions are calculated for each of the sea states in Table 4. We will use the numerical model for a random sea input, relying on equations (43-45) ,to calculate the tension power spectra of the final mooring design shown in Fig. 22. For the wave spectra, we use modified Pierson-Moskowitz spectra. This is conservative as fetch-limited spectra may be more appropriate. The tension spectra calculated in this manner are given in Fig. 24 and the standard deviations of the tension and average frequency are

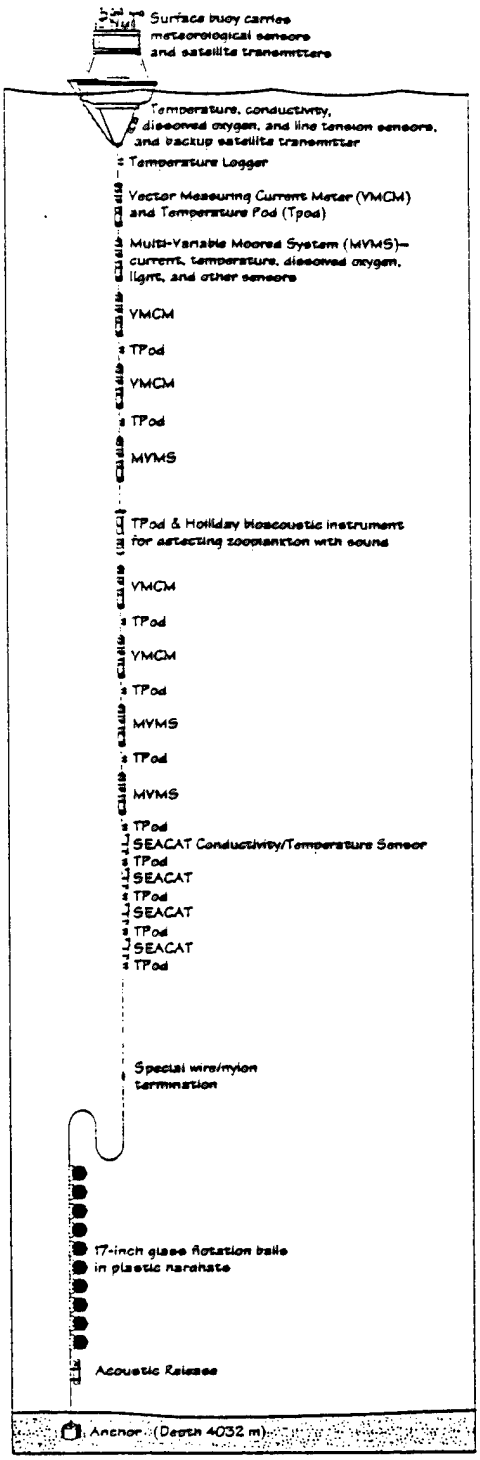

Figure 22: Schematic drawing of the 1995 Arabian Sea mooring.

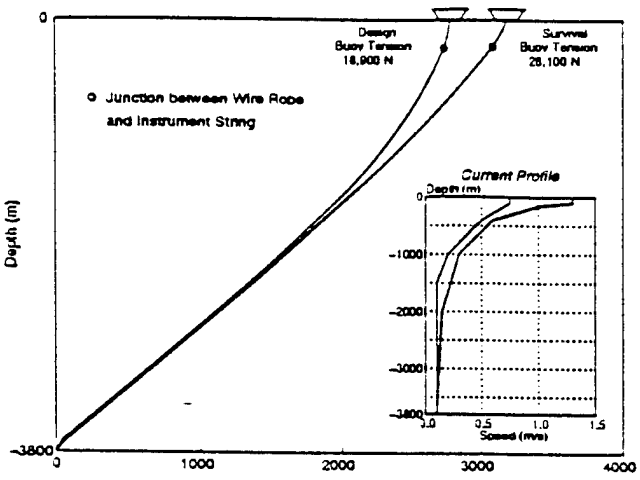

Figure 23: Static design and survival configurations for the Arabian Sea mooring.

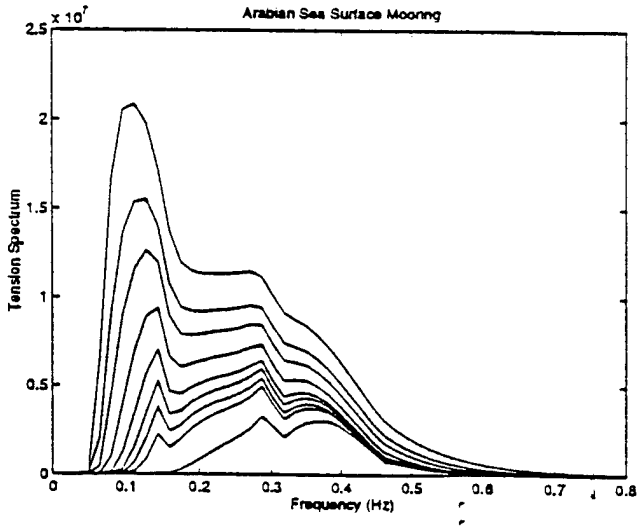

Figure 24: Tension power spectra at the top of the Arabian Sea Mooring corresponding to the sea states listed in Table 5.

Sea State	Design Current σ_T (N)	f_m (Hz)	Survival Current σ_T^s (N)
1	2240	0.391	—
2	2880	0.359	—
3	3100	0.349	—
4	3340	0.342	—
5	3570	0.332	—
6	3970	0.321	—
7	4410	0.308	—
8	4760	0.299	—
9	5250	0.288	5110

Table 5: Standard deviation and mean frequency of tensions at the top of the 1995 Arabian Sea surface mooring.

given in Table 5. We note that much of the preliminary dynamic analysis of the design of the Arabian Sea mooring was performed with the analytical model as the assumptions of nearly taut mooring line and instrument-string length less than 300 m apply.

The extreme dynamic tension is calculated using Equation (63) with the extreme standard deviation of $\sigma_T^s = 5110$ N corresponding to Sea State 9 and the survival current profile (last column of Table 5). We then determine the total extreme tension using Equation (64) with the extreme static tension of $T_o^s = 28,100$ N which corresponds to the survival current (Fig. 23). Thus,

$$\begin{aligned} T_{extreme} &= 28,100\,N + 3.85 \times 5110\,N \quad (71) \\ &= 52,700\,N \end{aligned}$$

The ultimate strength of a 3/4-inch shackle is 254,000 N. This represents a safety factor of 5.3 which easily satisfies the design constraints.

The fatigue analysis covers a six-month deployment (184 days). This corresponds to 16 million seconds or roughly five million cycles of loading. Using the probabilities in Tables 4, the average frequencies in Table 5 (corresponding to the design current), and Equation (68), we calculate the number of cycles corresponding to each sea state (column 1 in Table 6). The standard deviations in Table 5 along with the material fatigue constants represented by the dashed line in Fig. 20 (y=1.5 and q=3.7) are substituted into Equation (65) to give the damage per cycle for each sea state. The fraction of life lost due to the jth sea state

Sea State	Cycles	Galvanized Fraction Lost	Shot-Peened Fraction Lost
1	1.287×10^6	0.045	0.010
2	0.668×10^6	0.059	0.013
3	0.583×10^6	0.067	0.015
4	0.696×10^6	0.106	0.024
5	0.924×10^6	0.180	0.040
6	0.837×10^6	0.242	0.054
7	0.382×10^6	0.163	0.036
8	0.105×10^6	0.059	0.013
9	0.018×10^6	0.015	0.003
		Sum = 0.936	Sum = 0.208

Table 6: Summary of fatigue analysis for 3/4-inch galvanized and shot-peened shackles.

is given by Equation (69) (column 3 in Table 6). Summing these values gives the total fraction of life lost during the deployment. The value for the galvanized shackle is 0.936 which gives a safety factor of only 1.1 which is below the acceptable value of 4.0.

Going to a larger shackle was not an option because the shackle pin would not fit through the ends of the instruments and it would be too expensive to modify all of the instrument cages. The solution in this case was to use a shackle that was shot peened and painted with an corrosion-resistant coating. The ultimate strength of this part is the same as the galvanized component. The fatigue resistance of the shot-peened shackle, estimated from the data point in Fig. 20, is increased by 50%. Using fatigue constants of (y=2.25 and q=3.7), we recalculated the damage per cycle and the fraction of life lost due to the jth sea state (column 4 in Table 6). Summing these numbers gives a value for the shot-peened shackle of 0.208 which produces an acceptable safety factor of 4.8.

To analyze the strength and fatigue properties of the 3/8-inch wire rope, we take the static and dynamic tensions at the junction between the wire rope and the instrument string. In the numerical simulation this involves outputting the tension at the intersecting node. The extreme static tension corresponding to the survival current is 20,300 N. The extreme dynamic tension corresponding to Sea State 9 (and the survival-current mooring configuration) is found from the numerically calculated value for the standard deviation of the tension (last column of Table 7). The extreme total tension is then found from Equation (64):

$$T_{extreme} = 20,300\,N + 3.85 \times 1420\,N \quad (72)$$

Sea State	Design Current σ_T (N)	f_m (Hz)	Survival Current σ_T^s (N)
1	720	0.504	—
2	860	0.466	—
3	910	0.454	—
4	970	0.445	—
5	1020	0.432	—
6	1120	0.417	—
7	1230	0.400	—
8	1310	0.388	—
9	1430	0.374	1420

Table 7: Standard deviation and mean frequency of tensions in 3/8-Inch Wire Rope 1995 Arabian Sea Surface Mooring.

Sea State	Cycles	Fraction Lost
1	1.659×10^6	0.0004
2	0.867×10^6	0.0004
3	0.758×10^6	0.0005
4	0.906×10^6	0.0008
5	1.202×10^6	0.0013
6	1.087×10^6	0.0019
7	0.496×10^6	0.0013
8	0.136×10^6	0.0005
9	0.024×10^6	0.0001
Sum Fraction Lost =		0.0072

Table 8: Summary of fatigue analysis for 3/8-inch wire rope.

$$= 25,800\,N$$

In ultimate strength tests of 3/8-inch wire rope with swage fittings on the end, the wire breaks a few centimeters away from the swage joint with an average strength of 65,900 N. This represents a safety factor of 2.6 which satisfies the design constraints. Three hundred meters of 3/8-inch wire rope were eliminated from the original mooring design to achieve a safety factor above 2.5.

For fatigue analysis, we use the probabilities in Tables 4, the average frequencies in Table 7 (corresponding to the design current), and Equation (68) to determine the number of cycles corresponding to each sea state (column 1 in Table 8). The standard deviations in Table 7 (for the design current) along with the

material fatigue constants represented by the dashed line in Fig. 21 (y=2.4 and q=4.6) are substituted into equation (65) to give the damage per cycle for each sea state. The fraction of life lost due to the jth sea state is given by equation (69). Summing these values gives a total fraction of life lost during the deployment of only 0.0072 (Table 8). Thus, fatigue of the wire rope is not a concern.

The analysis of the shackle and the wire rope are examples where ultimate strength analysis (of the wire rope) and fatigue analysis (of the shackle) led to design changes. Similar analyses were performed on all mooring components including the instrument strength members. Fatigue results led to using oval-shaped links (instead of pear-shaped links) and strengthening the welds at the ends of the VMCM and MVMS instrument cages.

CONCLUSIONS

Dynamic analysis is key to designing oceanographic surface moorings for rough water environments. It is important in predicting both extreme loads and fatigue damage. We have presented a frequency domain numerical method and an analytical model that allow designers to perform these calculations in different sea states and have shown how to incorporate the results into ultimate strength and fatigue analysis.

The analytical model described in Section 3 is useful in the early stages of design because it shows explicitly the individual effects of the instruments, mooring hardware, wire rope and synthetic rope that go into the overall dynamic response. It is orders of magnitude faster than numerical simulations, and gives accurate results for moorings with the instruments concentrated in the top portion of the mooring.

Hydrodynamic coefficients and wave exciting forces of different shaped oceanographic buoys are given along with the material and fatigue parameters for the components and instruments that make up the mooring line and instrument strings. These are used with the results from static and dynamic analysis to predict if a mooring will survive a deployment. The case study of the Arabian Sea surface mooring shows how the design techniques presented in this paper can isolate weaknesses and lead to improve designs in terms of ultimate strength and fatigue resistance.

ACKNOWLEDGEMENTS

Funding for this research was provided by the Office of Naval Research under grants N00014-92-J-1269 and N00014-93-1-0704.

APPENDIX

The following tables give important parameters of oceanographic instruments used on the 1991 *Marine-Light Mixed-Layer* mooring and the 1995 *Arabian Sea* mooring. These values are used for the static and dynamic calculations presented in this paper.

In the tables, *Type* corresponds to the the method of attachment. *Open Cage* uses a structural frame of 3/4-inch stainless-steel rod with the instrument suspended inside the frame. Examples of this are the VMCM and ADCP shown in Fig. 2. *Side-Mounted on Rod* corresponds to the instrument housing clamped to a single piece of 1-1/4-inch diameter stainless-steel rod which acts as the strength member. An example of this is the SEACAT shown in Fig. 2. *In-Line Cylinder* corresponds to a cylinder pressure housing with attachment points mounted on the end caps so that pressure housing becomes the structural member of the mooring line. An example of this is the engineering instrument that measures mooring-line tension. *Clamp to Mooring Line* uses a clamp that hold the instrument in place on the mooring line by friction.

The added mass and drag coefficients are estimates made by the authors. The drag coefficient is assumed to be the same for both vertical and transverse motion.

Table A1
Vector Measuring Current Meter (VMCM)

Type	Open Cage
Length	2.9 m
Mass	81 kg
Weight in Water	495 N
Vertical Added Mass	20 kg
Transverse Added Mass	33 kg
Vertical Projected Area	0.09 m^2
Transverse Projected Area	0.56 m^2
Drag Coefficient	1.0

Table A2
Multi-Variable Moored System (MVMS)

Type	Open Cage
Length	2.9 m
Mass	94.6 kg
Weight in Water	581 N
Vertical Added Mass	21 kg
Transverse Added Mass	35 kg
Vertical Projected Area	0.10 m^2
Transverse Projected Area	0.68 m^2
Drag Coefficient	1.0

Table A3
Acoustic Doppler Current Profiler (ADCP)

Type	Open Cage
Length	2.3 m
Mass	107 kg
Weight in Water	516 N
Vertical Added Mass	27 kg
Transverse Added Mass	54 kg
Vertical Projected Area	0.26 m^2
Transverse Projected Area	0.93 m^2
Drag Coefficient	1.0

Table A4
SEACAT

Type	Side-Mounted on Rod
Length	2.0 m
Mass	18 kg
Weight in Water	112 N
Vertical Added Mass	0.5 kg
Transverse Added Mass	6.6 kg
Vertical Projected Area	0.01 m^2
Transverse Projected Area	0.05 m^2
Drag Coefficient	1.0

Table A5
Bio-Optical Moored System (BOMS)

Type	Side-Mounted on Rod
Length	2.9 m
Mass	61.5 kg
Weight in Water	305 N
Vertical Added Mass	4.5 kg
Transverse Added Mass	25 kg
Vertical Projected Area	0.03 m^2
Transverse Projected Area	0.15 m^2
Drag Coefficient	1.0

Table A6
Custom-Made Bio-Optical Sensor (MOORDEX)

Type	Custom-Made Attachment
Length	2.0 m
Mass	157 kg
Weight in Water	979 N
Vertical Added Mass	51 kg
Transverse Added Mass	32 kg
Vertical Projected Area	0.29 m^2
Transverse Projected Area	0.19 m^2
Drag Coefficient	0.8

Table A7
Holliday Bio-Acoustic Instrument

Type	Open Cage
Length	2.9 m
Mass	138 kg
Weight in Water	1030 N
Vertical Added Mass	20 kg
Transverse Added Mass	33 kg
Vertical Projected Area	0.09 m^2
Transverse Projected Area	0.56 m^2
Drag Coefficient	1.0

Table A8
Temperature Pod Sensors (TPod)

Type	Clamp to Mooring Line
Length	0.5 m
Mass	4.5 kg
Weight in Water	35.6 N
Vertical Added Mass	0.6 kg
Transverse Added Mass	4.0 kg
Vertical Projected Area	0.01 m^2
Transverse Projected Area	0.05 m^2
Drag Coefficient	1.0

Table A9
Engineering Instrument

Type	In-Line Cylinder
Length	1.0 m
Mass	40 kg
Weight in Water	225 N
Vertical Added Mass	2.0 kg
Transverse Added Mass	19 kg
Vertical Projected Area	0.02 m^2
Transverse Projected Area	0.08 m^2
Drag Coefficient	1.0

REFERENCES

BERTEAUX, H.O. 1976 *Buoy Engineering* John Wiley and Sons, Inc., New York.

BERTEAUX, H.O. 1991 *Coastal and Oceanic Buoy Engineering* Published by H.O. Berteaux, Woods Hole, MA. 1991.

BERTEAUX, H.O. and ROY, R.L. 1986 Wave Tank Study Of Moored Buoy Hulls For Air-sea Interaction Applications *IEEE Oceans '86 Conf. Proc.*, Washington, D.C., pp. 259-270.

BERTEAUX, H.O. and WALDEN, R.G. 1970 An Engineering Program to Improve the Reliability of Deep Sea Moorings Technical Report, Woods Hole Oceanographic Institution, Woods Hole, MA, Ref. No. 70-48.

BLIEK, A. 1984 Dynamic Analysis of Single Span Cables, Ph.D. thesis, Massachusetts Institute of Technology, Cambridge, MA.

BRESLIN, J.P. 1974 Dynamic Forces Exerted by Oscillating Cables *J. Hydronautics*, Vol. 8, pp. 18-31.

BRISCOE, M.G. and WELLER, R.A. 1984 Preliminary Results From The Long Term Upper Ocean Study (LOTUS) *Dynamics of Atmospheres and Oceans*, Vol. 8, pp. 243-265.

CANADA, R.H. and MAY, D.R. 1985 Mooring Developments and Design Philosophy at the National Data Buoy Center *IEEE Oceans '85 Conf. Proc.*, San Diego, California, pp. 1336-1343.

CAUGHEY, T.K. 1963 Equivalent Linearization Techniques *J. Acoustic Soc. Am.*, Vol. 35, pp. 1706-1711.

COLLINS, J.A. 1993 *Failure of Materials in Mechanical Design*, John Wiley and Sons, Inc., New York.

FALTINSEN, O.M. 1990 *Sea Loads on Ships and Offshore Structures*, Cambridge University Press, Cambridge, UK.

FORSYTHE, G.E., MALCOLM, M.A., and MOLER, C.B. 1977 *Computer Methods for Mathematical Computations*, Prentice-Hall, Inc., New Jersey.

GARRETT,C.J.R. 1970 Bottomless Harbors *J. Fluid Mechanics*, Vol. 43, pp. 433-449.

GARRETT, C.J.R. 1971 Wave Forces On A Circular Dock *J. Fluid Mechanics*, Vol. 46, pp. 129-139.

GOODMAN, T.R., KAPLAN, P., SARGENT, T.P., and BENTSON, J. 1972 Static and Dynamic Analysis of a Moored Buoy System, Technical Report, National Data Buoy Center, Stennis Space Center, MS, Ref. No. NDBCM 6113.1.

GOODMAN, T.R. and BRESLIN, J.P. 1976 Statics and Dynamics of Anchoring Cables in Waves *J. Hydronautics*, Vol. 10, pp. 113-120.

GROSENBAUGH, M.A., YOERGER, D.R., HOVER, F.S., and TRIANTAFYLLOU, M.S. 1991 Drag Forces and Vortex-Induced Vibrations of a Long Vertical Tow Cable. Part II: Unsteady Towing Conditions *J. Offshore Mech. Arctic Engng.* Vol. 113, pp. 117-127.

GROSENBAUGH, M.A. 1995a The Effect of Hydrodynamic Damping on the Tension of Oceanographic Surface Moorings *Proceedings International Symposium on Cable Dynamics, Leige, Belgium.*

GROSENBAUGH, M.A. 1995b On the Dynamics of Oceanographic Surface Moorings *Ocean Engng.*, to appear.

GROSENBAUGH, M.A. 1995c Designing Oceanographic Surface Moorings To Withstand Fatigue J. Atmos. Oceanic. Technol., to appear.

KIM, Y.H, VANDIVER, J.K., and HOLLER, R. 1986 Vortex-Induced Vibration and Drag Coefficients of Long Cables Subjected to Sheared Flow *J. of Energy Resources Technology*, Vol. 108.

KOKKINOWRACHOS, K., MAVRAKOS, S.A., and ASORAKOS, S. 1986 Behavior Of Vertical Bodies Of Revolution In Waves *Ocean Engng.*, Vol. 13, pp. 505-538.

MAVRAKOS, S.A. 1985 Wave Loads On A Stationary Floating Bottomless Cylindrical Body With Finite Wall Thickness *Applied Ocean Research*, Vol. 7, pp. 213-224.

MAVRAKOS, S.A. 1988 Hydrodynamic Coefficients For A Thick-walled Bottomless Cylindrical Body Floating In Water Of Finite Depth *Ocean Engng.*, 15,

pp. 213-229.

MEI, C.C. 1983 *The Applied Dynamics of Ocean Surface Waves*, John Wiley & Sons, New York.

MESERVE, J.M. 1974 *U.S. Navy Marine Climatic Atlas of the World Volume I North Atlantic Ocean NAVAIR 50-1C-528*, U.S. Government Printing Office, Washington D.C..

MILBURN, H.B. and MCCLAIN, P.D. 1986 ATLAS - A Low Cost Satellite Data Telemetry Mooring Developed for NOAA's Climate Research Mission *Proceedings of the International Buoy Technology Symposium, New Orleans.*

MILOH, T. 1983 Wave Loads On A Floating Solar Pond *Proc. Int. Workshop on Ship and Platform Motions*, Berkeley, CA, pp. 110-131.

MINER, M.A. 1945 Cumulative Damage in Fatigue *Trans. ASME Series E, J. Applied Mech.*, Vol. 67, pp. A159-A164.

NEWMAN, J.N. 1977 The Motions Of A Floating Slender Torus *J. Fluid Mechanics*, Vol. 83, pp. 721-735.

PAULLING, J.R. 1979 An Equivalent Linear Representation of the Forces Exerted on the OTEC Cold-Water Pipe by the Combined Effects of Waves and Currents in *Ocean Engineering for OTEC*, published by ASME, Griffin and Giannotti (editors).

PLUEDDEMANN, A.J., WELLER, R.A., STRAMSKA, M., DICKEY, T.D., and MARRA, J. 1995 The Vertical Structure of the Upper Ocean During the Marine Light-Mixed Layers Experiment, *J. Geophys. Res.*, Vol. 100(C4), pp. 6605-6619.

RICHARDSON, W.S., STIMSON, P.B., and WILKINS, C.H. 1963 Current Measurements from Moored Buoys, *Deep Sea Research*, Vol. 10, pp. 369-388.

TRIANTAFYLLOU, M.S. 1987 Dynamics of Cables and Chains *The Shock and Vibrations Digest*, Vol. 19, pp. 3-5.

TRIANTAFYLLOU, M.S, BLIEK, A., and SHIN, H. 1986 Static and Fatigue Analysis of Multi-Leg Mooring System, Tech. Rep. MITSG Ref. 86-21, Massachusetts Inst. of Tech., Cambridge, Massachusetts, pp. 75.

TRIANTAFYLLOU, M.S., BLIEK, A., BURGESS, J., and SHIN, H. 1987 Mooring Dynamics for Offshore Applications, Part I", Technical Report, MIT Sea Grant, Cambridge, MA, Ref. No. MITSG 86-1.

WELLER, R.A. and DAVIS, R.E. 1980 A Vector Measuring Current Meter *Deep Sea Research*, Vol. 27A, pp. 565-582.

WELLER, R.A., RUDNICK, D.L., PENNINGTON, N.J., TRASK, R.P., and VALDES, J.R. 1990 Measuring Upper Ocean Variability from an Array of Surface Moorings in the Subtropical Convergence Zone *J. Atmos. Oceanic. Technol.*, Vol. 7, pp. 68-84.

WHITE, F.M. 1974 *Viscous Fluid Flow*, McGraw-Hill, Inc., New York.

YEUNG, R.W. 1981 Added Mass And Damping Of A Vertical Cylinder In Finite Depth Waters *Applied Ocean Research*, Vol. 3, pp. 119-133.